OPEN ACCESS
Journal of Innovative Optical Health Sciences
(2026) 2630018 (34 pages)

DOI: 10.1142/S1793545826300181

World Scientific
www.worldscientific.com

Enhancement strategies for stimulated Raman scattering microscopy

Yingjie He, Qingjun Meng and Minbiao Ji*
State Key Laboratory of Surface Physics
and Department of Physics
Shanghai Key Laboratory of Metasurfaces for Light Manipulation
Endoscopy Center and Endoscopy Research Institute
Zhongshan Hospital, Fudan University
Shanghai 200433, P. R. China
**minbiaoj@fudan.edu.cn*

Received 18 June 2026
Accepted 9 August 2026
Published 8 September 2026

Stimulated Raman scattering (SRS) microscopy has emerged as a powerful chemical imaging platform that translates molecular bond vibrations into rapid visualization of biomolecules, metabolites, and drugs. As SRS moves from proof-of-concept imaging toward live cell analysis, thick tissue interrogation, biochemical readout, and computational histopathology, its further development is increasingly limited by coupled trade-offs among sensitivity, acquisition speed, spectral bandwidth, penetration depth, spatial resolution, and interpretability. This review summarizes recent advances in enhancement strategies for SRS microscopy through four interconnected dimensions: signal, acquisition, light-field, and information engineering. Signal enhancement improves the detectability of weak Raman responses, acquisition enhancement increases imaging throughput and spectral accessibility, light-field enhancement extends SRS toward deep, volumetric, and super-resolution imaging, and information enhancement expands SRS from chemical mapping to multidimensional molecular analysis. Through this framework, we highlight how these enhancement strategies are enabling SRS microscopy to evolve into a more sensitive, faster, deeper, and more interpretable molecular imaging platform for biology, pathology, and precision medicine.

Keywords: Stimulated Raman scattering microscopy; enhancement strategies; molecular imaging.

*Corresponding author.

1. Introduction

Stimulated Raman scattering (SRS) microscopy has emerged as a powerful chemical imaging modality for biological and biomedical research.[1,2] By converting intrinsic molecular vibrations into image contrast, SRS enables rapid visualization of endogenous biomolecules, metabolic activities, and exogenous compounds without fluorescent labeling.[3,4] Compared with spontaneous Raman microscopy, SRS achieves much higher imaging speed and sensitivity through coherent excitation and high-frequency phase-sensitive detection, while retaining the molecular specificity of vibrational spectroscopy.[5] These capabilities have supported broad applications in live-cell imaging, metabolic analysis, drug delivery, tissue histology, and biomedical diagnosis, and have continued to motivate efforts to improve the performance and usability of SRS microscopy.[6–10]

Despite these advances, conventional SRS microscopy still faces several key limitations. At the signal level, the SRS response appears as a weak intensity modulation on a strong laser background, making it vulnerable to high-frequency laser intensity noise, shot noise, and non-Raman backgrounds.[11–13] At the acquisition level, faster imaging or higher throughput often requires shorter pixel dwell time, reduced spectral sampling, or simplified laser operation, which can compromise signal-to-noise ratio (SNR), chemical specificity, or system stability.[14–16] At the light-field level, scattering, aberration, and signal attenuation in thick or heterogeneous specimens limit penetration depth, optical sectioning, spatial resolution, and volumetric imaging performance.[17,18] At the information level, single-frequency or intensity-based SRS measurements may not fully resolve subtle molecular states, structural heterogeneity, molecular orientation, or clinically relevant tissue features.[19–21] These limitations indicate that the next stage of SRS development requires enhancement strategies that improve not only sensitivity, but also acquisition efficiency, light-field control, and multidimensional information readout.

In response to these challenges, recent enhancement strategies are forming an integrated framework for improving how vibrational signals are generated, acquired, delivered, and interpreted. Signal enhancement aims to increase the strength and detectability of weak Raman responses through improved laser stability, modulation and detection schemes, background suppression, resonance or field enhancement, and computational denoising.[22–24] Acquisition enhancement seeks to improve imaging speed, throughput, spectral access, and system robustness by using fast scanning, multiplex or hyperspectral acquisition, sparse sampling, computational reconstruction, and compact laser platforms.[25,26] Light-field enhancement manipulates excitation and detection fields to improve penetration depth, spatial resolution, axial encoding, and volumetric imaging, including strategies based on Bessel beams, tomography, phase control, adaptive optics, and super-resolution SRS.[27,28] Information enhancement further expands SRS from selected-band chemical mapping toward multidimensional molecular analysis by incorporating spectral unmixing, biochemical readout, polarization and tensor information, computational reconstruction, and artificial intelligence (AI)-assisted interpretation.[19,29]

These four dimensions are intended as interconnected operational categories rather than mutually exclusive mechanistic classes. The primary placement of a strategy is determined by two considerations: the stage of the SRS imaging pathway at which its dominant intervention occurs and the principal limitation it is designed to address. Signal enhancement primarily acts on Raman-response generation, detection, noise-floor reduction, alternative vibrational readout, or recovery of physically recorded weak contrast; acquisition enhancement acts on sampling, tuning, encoding, parallelization, and measurement efficiency; light-field enhancement acts on optical-field delivery, propagation, spatial response, image formation, and collection; and information enhancement transforms acquired SRS measurements into compositional, structural, spatial, functional, representational, or decision-level variables. Because hybrid platforms often improve several performance metrics simultaneously, secondary benefits and cross-category couplings are discussed explicitly rather than used to determine primary placement.

In this paper, we summarize major enhancement strategies for SRS microscopy through four interconnected themes: signal enhancement, acquisition enhancement, light-field enhancement, and information enhancement. Rather than providing a

general survey of SRS principles, instrumentation, and applications, we focus on how different enhancement strategies address the key trade-offs among sensitivity, imaging speed, spectral bandwidth, penetration depth, spatial resolution, molecular specificity, and interpretability. We first discuss methods that improve signal generation and detection, followed by approaches that increase acquisition efficiency and system accessibility. We then review light-field engineering strategies for deep, volumetric, and super-resolution SRS imaging, as well as information-oriented methods that enable hyperspectral, structural, polarization-resolved, AI-assisted, and clinically interpretable molecular readout. Finally, we discuss the remaining challenges and future perspectives for developing SRS microscopy into a more sensitive, faster, deeper, and more informative molecular imaging platform (Fig. 1).

2. Principles and Performance Metrics for Evaluating SRS Enhancement Strategies

Before discussing specific enhancement strategies, it is useful to briefly define the basic signal pathway, instrumental configuration, and performance metrics of conventional SRS microscopy. This section is not intended to provide a comprehensive tutorial on SRS principles, which has been covered in previous reviews. Instead, it establishes the technical baseline from which signal, acquisition, light-field, and information enhancement strategies can be understood.

2.1. *Basic signal generation and detection*

In a typical SRS microscope, two synchronized laser beams, referred to as the pump beam and the Stokes

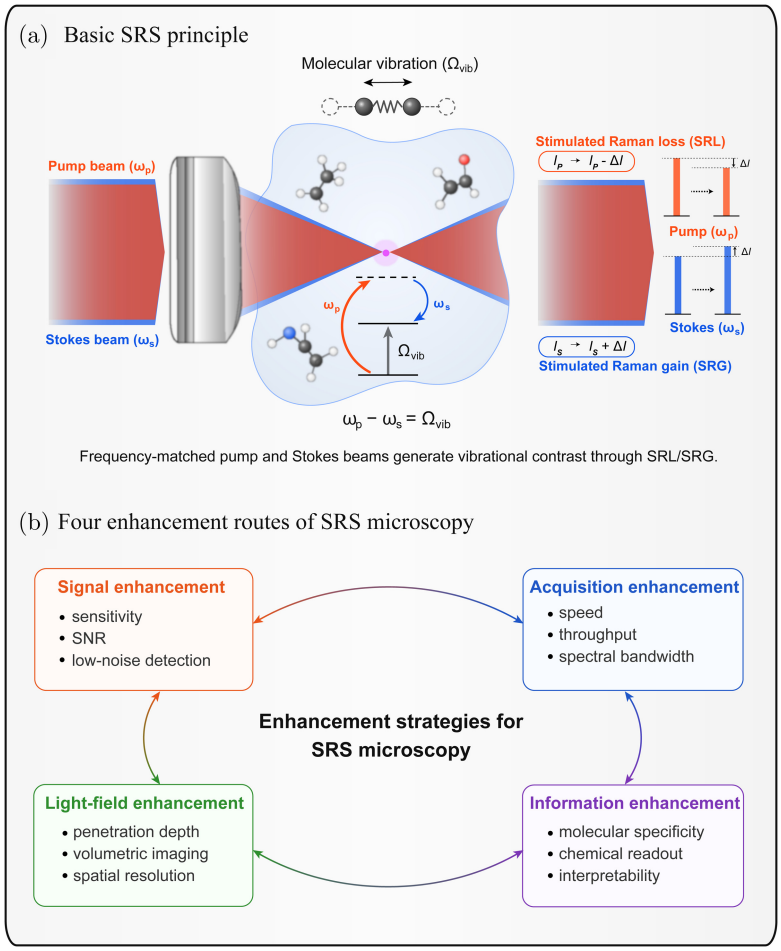

Fig. 1. Conceptual framework of enhancement strategies for SRS microscopy. (a) Basic principles of SRS signal generation. (b) Four interconnected enhancement routes of SRS microscopy.

beam, are spatially and temporally overlapped at the focal volume of a microscope objective. When the frequency difference between the two beams matches a molecular vibrational frequency, coherent energy transfer occurs between the optical fields and the molecular vibration (Fig. 1(a)). This process leads to a small intensity loss in the pump beam, known as stimulated Raman loss (SRL), and a corresponding intensity gain in the Stokes beam, known as stimulated Raman gain (SRG).[30–32] By tuning the frequency difference between the pump and Stokes beams, SRS microscopy can selectively image molecular vibrations associated with chemical bonds such as C–H, C–D, C≡C, C≡N, O–H, and amide modes.[33–36]

A central advantage of SRS microscopy is that its signal is directly related to the imaginary part of the third-order nonlinear susceptibility associated with the molecular vibration.[37,38] As a result, the SRS spectrum generally follows the line shape of spontaneous Raman scattering and is linearly proportional to molecular concentration under standard imaging conditions.[12,39] This linear concentration dependence distinguishes SRS from coherent anti-Stokes Raman scattering, where nonresonant background and more complex signal scaling can complicate quantitative interpretation.[40–43] Therefore, SRS is particularly attractive for quantitative chemical imaging of biological specimens, including lipids, proteins, metabolites, drugs, and isotope-labeled molecules.[44–46]

However, the same detection mechanism that enables fast chemical imaging also creates a major sensitivity challenge. The SRS signal is not detected as newly generated light at a distinct wavelength, but as a weak intensity modulation imposed on a strong pump or Stokes beam. In many biological imaging conditions, this fractional modulation is extremely small and can be easily obscured by laser intensity noise, shot noise, electronic noise, and other non-Raman backgrounds. To extract this weak modulation, one beam is typically intensity-modulated at a high frequency, and the induced modulation transfer to the other beam is detected with a photodiode and a lock-in amplifier. This high-frequency, phase-sensitive detection scheme suppresses low-frequency laser noise and enables rapid label-free vibrational imaging, but it also defines the noise floor that many signal-enhancement strategies seek to overcome.

2.2. *Standard instrumentation and acquisition modes*

A conventional SRS microscope usually consists of a synchronized dual-wavelength laser source, a modulation unit, a beam-combining and scanning module, a microscope platform, photodetectors, and phase-sensitive electronics. The pump and Stokes beams are typically derived from synchronized picosecond or femtosecond laser sources, with one beam modulated by an electro-optic modulator, acousto-optic modulator, or other high-frequency modulation device. After being spatially combined, the beams are focused into the sample through a high-numerical-aperture objective. The transmitted or reflected light is then collected, filtered to remove the modulated beam when needed, and sent to a photodetector for lock-in demodulation. This architecture provides the basis for most point-scanning SRS microscopes and can be adapted for forward detection, epi-detection, hyperspectral imaging, and multimodal nonlinear optical imaging.[47,48]

Different acquisition modes offer different balances between speed, spectral information, sensitivity, and system complexity. Single-frequency or narrowband SRS is the most widely used mode for fast imaging of selected vibrational bands. It provides high imaging speed and relatively high sensitivity, making it suitable for live-cell imaging, lipid mapping, isotope tracing, and rapid tissue assessment. Its limitation is that it only samples one or a few Raman shifts, which may be insufficient for distinguishing spectrally overlapping molecular species or resolving subtle biochemical heterogeneity.

Hyperspectral SRS addresses this limitation by acquiring an image stack over a range of Raman shifts, thereby providing a vibrational spectrum at each pixel. This approach enables spectral unmixing, multicomponent chemical mapping, and more quantitative molecular analysis. However, hyperspectral imaging typically requires wavelength scanning, delay scanning, multiplex detection, or broadband excitation, which can increase acquisition time, optical complexity, and data-processing demand.[49,50] Spectral focusing, in which chirped femtosecond pulses are used to encode Raman shifts through temporal delay, has become an important strategy for accelerating hyperspectral SRS while retaining chemical specificity.[14,51] Other

approaches, including broadband SRS, time-encoded Raman acquisition, multicolor SRS, and rapidly tunable fiber-laser systems, further expand the acquisition landscape and motivate the development of acquisition-enhanced SRS microscopy.[16,52–54]

2.3. *Performance metrics, classification principles, and trade-offs*

For the purpose of this review, enhancement of SRS microscopy can be understood as a set of strategies that reshape the performance trade-offs of conventional SRS. The most direct metric is signal-to-noise ratio, which determines whether weak vibrational contrast can be reliably detected. Closely related metrics include detection limit, modulation depth, laser noise suppression, and background rejection. These parameters are central to signal enhancement, where the goal is to increase the absolute Raman response, reduce the noise floor, or convert the SRS response into a more detectable signal.

A second group of metrics concerns acquisition performance. These include pixel dwell time, frame rate, spectral sampling rate, field of view, throughput, and long-term system stability. In many biological applications, such as live-cell metabolic imaging or high-throughput cellular screening, the limiting factor is not only whether a signal can be detected, but whether it can be detected fast enough and reproducibly enough to capture dynamic or statistically meaningful biological processes. Acquisition enhancement therefore focuses on increasing the amount of reliable chemical information obtained per unit time, while maintaining acceptable light dose and system robustness.

A third group of metrics relates to spatial light delivery and image formation. Penetration depth, optical sectioning, spatial resolution, volumetric imaging capability, and robustness against scattering and aberration are particularly important for thick tissues, organoids, and clinical specimens. Conventional point-scanning SRS performs well in thin or transparent samples but can be limited by scattering-induced signal attenuation, wavefront distortion, and out-of-focus background in complex specimens. Light-field enhancement addresses these problems by engineering excitation beams, detection geometries, wavefronts, or nonlinear optical responses to improve depth, resolution, and three-dimensional imaging capability.

A fourth group of metrics describes molecular information content. These include spectral resolution, spectral bandwidth, chemical specificity, molecular orientation sensitivity, structural sensitivity, multimodal contrast, and computational interpretability. Conventional single-frequency SRS provides strong chemical contrast but limited information bandwidth. By contrast, hyperspectral, polarization-resolved, tensor-sensitive, multimodal, and computationally reconstructed SRS approaches can extract richer molecular and structural information from the same sample. Information enhancement therefore extends SRS beyond intensity-based chemical mapping toward multidimensional molecular readout.

Because these performance metrics are strongly coupled, the present framework does not classify a strategy solely according to its final performance outcome. Instead, primary placement is determined by the stage of the SRS imaging pathway at which the dominant intervention occurs and the principal limitation or design objective it addresses. Hybrid approaches may therefore improve multiple metrics across several dimensions; such secondary benefits are treated as cross-category effects and are discussed or cross-referenced where relevant. Detailed operational definitions, inclusion criteria, primary performance metrics, and representative cross-category examples are summarized in Supplementary Table S1. Representative quantitative benchmarks for selected strategies across the four enhancement dimensions are further summarized in Supplementary Table S2. Because these values were obtained using different molecular targets, specimens, optical parameters, acquisition settings, and evaluation criteria, they are presented to illustrate reported performance ranges and associated trade-offs rather than to establish a direct ranking among methods.

These performance metrics are strongly coupled. Increasing laser power can improve signal strength but may aggravate photodamage or phototoxicity. Shortening pixel dwell time can increase imaging speed but may reduce signal-to-noise ratio. Expanding spectral coverage can improve molecular specificity but often increases acquisition time and computational burden. Improving penetration depth may require trade-offs in spatial resolution, collection efficiency, or optical complexity. Therefore, enhancement of SRS microscopy should not be viewed as a simple pursuit of a single optimized parameter. Rather, it represents a coordinated

effort to balance sensitivity, speed, depth, resolution, specificity, dose, and information bandwidth for specific biological and biomedical tasks (Fig. 1(b)).

3. Signal Enhancement: Improving Sensitivity and Detectability

Signal enhancement is the most direct route for expanding the applicability of SRS microscopy to weakly scattering molecules, low-abundance species, and low-dose biological imaging. In conventional SRS, molecular vibrational contrast is detected as a small intensity modulation on a strong pump or Stokes beam. Although high-frequency modulation and phase-sensitive detection have enabled rapid and quantitative chemical imaging, the detectable signal can still be limited by laser intensity noise, shot noise, electronic noise, non-Raman backgrounds, and the intrinsically small Raman cross-sections of many biomolecules. These limitations become particularly important when imaging dilute metabolites, small-molecule drugs, weak Raman probes, or nanoscale biochemical events under biologically compatible illumination conditions.

Signal-enhancement strategies span several technical families and are not strictly mutually exclusive, because individual platforms may integrate molecular, optical, electronic, and computational mechanisms. For clarity, we organize these strategies according to their dominant technical family and implementation pathway rather than imposing a strictly mechanism-exclusive classification. First, hardware noise suppression and algorithm-assisted denoising improve the extraction of weak SRS contrast, either by reducing technical noise and non-Raman backgrounds during acquisition or by enhancing the visibility of physically recorded weak signals after acquisition.[24,55–60] Second, electronic resonance, excitation-wavelength engineering, molecular-probe design, and plasmonic local-field enhancement strengthen the generated Raman response or improve its effective detectability.[22,61–67] Third, stimulated Raman photothermal (SRP) microscopy converts Raman-resonant energy deposition into a thermally mediated optical signal, providing an alternative to direct SRL or SRG detection.[68–70] Finally, quantum-enhanced and emerging photonic approaches employ nonclassical light, resonant field buildup, optical confinement, or engineered photonic modes to extend SRS beyond conventional free-space excitation and detection architectures.[71–75] These categories therefore serve as an organizational framework for major technical routes rather than as strictly exclusive physical mechanisms, and hybrid methods that combine multiple enhancement principles are noted explicitly where relevant (Fig. 2). Depending on the enhancement mechanism, representative performance metrics include SNR or contrast-to-noise ratio, detection limit, fractional modulation depth, noise and background suppression, and dose- or time-normalized sensitivity.

3.1. *Noise suppression and algorithm-assisted weak-signal extraction*

Noise suppression and algorithm-assisted weak-signal extraction constitute a major technical family of SRS signal enhancement. Both aim to recover weak SRL or SRG contrast from dominant measurement noise, although they operate at different stages of the imaging workflow. Hardware approaches improve measurement fidelity during acquisition by suppressing laser intensity fluctuations, detector noise, non-Raman backgrounds, and other technical noise sources. Computational approaches operate after acquisition and exploit spatial, spectral, or learned priors to improve the visibility and usability of weak information already encoded in the measured data. Algorithmic denoising therefore complements, rather than replaces, physical low-noise detection.

High-frequency modulation and phase-sensitive detection provide the basic architecture for sensitive SRS measurements. By modulating one beam at megahertz frequencies and demodulating the transferred modulation on the other beam with a lock-in amplifier, SRS detection can be shifted away from the low-frequency regime in which laser technical noise is typically strongest. This approach enabled rapid label-free vibrational imaging and established the conventional detection architecture on which subsequent optimization of laser sources, modulation schemes, photodetectors, and detection electronics has been built.

Shot-noise-limited SRS detection represents an important benchmark for hardware-based signal enhancement. In this regime, technical noise from

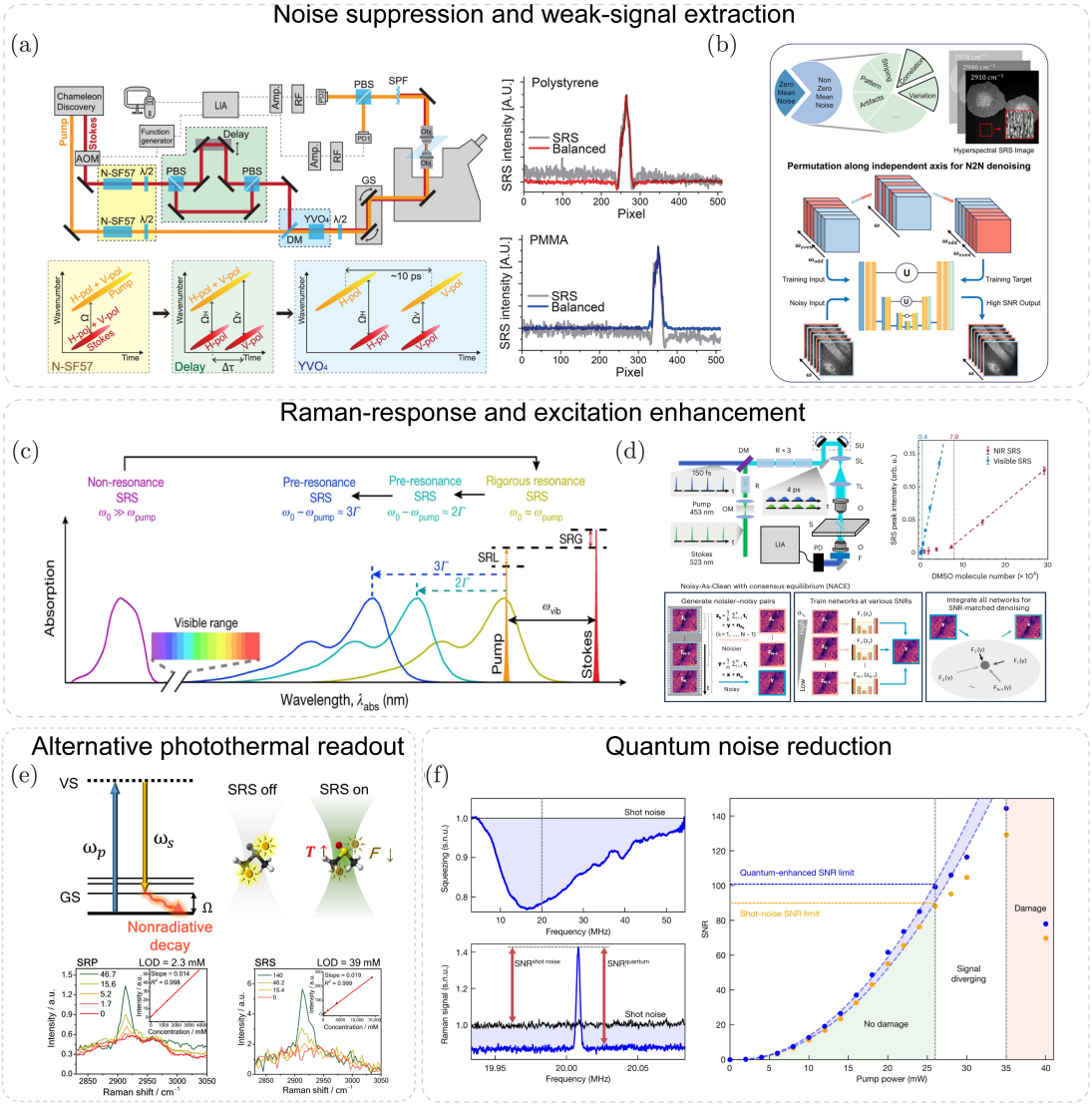

Fig. 2. Representative signal-enhancement strategies organized by their dominant mechanisms. (a) and (b) Noise suppression and weak-signal extraction through two-color balanced detection and self-supervised hyperspectral denoising. Adapted with permission from Ref. 78 and reproduced with permission from Ref. 60, respectively. (c) and (d) Raman-response and excitation enhancement through electronic pre-resonance and URV-SRS integrating visible excitation, pulse chirping, denoising, and Fourier reweighting. Reproduced with permission from Ref. 22 and adapted with permission from Ref. 63, respectively. (e) SRP microscopy converts vibrational excitation into a photothermal readout. Adapted with permission from Ref. 68. (f) Quantum-enhanced nonlinear microscopy reduces the measurement noise floor using quantum-correlated light under photodamage-limited conditions. Adapted with permission from Ref. 71.

the laser source and detection electronics is suppressed sufficiently that the remaining measurement noise is dominated by photon shot noise. Achieving this condition requires stable synchronized laser sources, appropriate modulation frequencies, low-noise photodetectors, and careful optimization of optical power and detector operation.[57,76,77] The shot-noise-limited regime therefore provides the classical physical benchmark against which subsequent noise-suppression and quantum-enhanced detection strategies should be evaluated.

Balanced detection further improves SRS sensitivity by suppressing common-mode laser intensity fluctuations. In a typical balanced scheme, a reference beam is used to subtract correlated intensity noise from the signal channel, allowing weak SRL or SRG modulation to be recovered with higher fidelity. Variants of this concept have been developed to improve compatibility with different laser sources

and imaging configurations. For example, in-line balanced detection uses a birefringent element to generate a time-delayed, polarization-multiplexed collinear reference beam, so that the signal and reference experience similar optical paths through the sample.[56] Two-color balanced detection extends this idea by allowing two SRS channels to act as mutual intensity references, thereby reducing background noise toward the shot-noise limit even in fiber-based femtosecond laser systems (Fig. 2 (a)).[78] Importantly, balanced detection suppresses common-mode technical noise and enables an otherwise noise-limited system to approach or reach the shot-noise limit; it does not, by itself, reduce photon shot noise below the standard quantum limit. Such schemes are particularly valuable for compact or fiber-laser-based SRS microscopes, where laser relative intensity noise can otherwise limit sensitivity.[55]

Complementary to balanced detection, modulation engineering provides another hardware route for improving weak-signal extraction and background rejection. Nyquist modulation uses the repetition structure of a two-branch ultrafast fiber source to achieve stable high-frequency modulation and shot-noise-limited SRS detection.[79] Frequency-modulation SRS (FM-SRS), in contrast, targets parasitic non-Raman backgrounds by exploiting their weaker spectral dependence compared with the vibrationally resonant SRS signal.[80] By modulating the excitation frequency or switching between nearby Raman shifts, FM-SRS can suppress unwanted background contributions while preserving chemically specific SRS contrast.[81,82] These approaches demonstrate that the modulation format itself can be used as an active tool for enhancing SRS detectability, rather than simply serving as a lock-in reference.

In parallel with hardware optimization, computational denoising has become an increasingly important post-acquisition strategy for improving weak SRS contrast.[83] Early deep-learning approaches used supervised image-to-image restoration, in which low-SNR SRS images were mapped to high-SNR references acquired with longer dwell time or higher signal averaging. U-Net-based denoising provided a representative example, showing that convolutional neural networks can substantially improve low-SNR SRS images and generalize across different imaging powers, depths, zoom factors, and sample geometries.[24] These methods are useful when increasing laser power or acquisition time is undesirable because of photodamage, phototoxicity, or sample dynamics. Their reliability, however, depends on whether physically meaningful signal information remains encoded in the noisy measurement.

For hyperspectral SRS, the denoising problem is more complex because the noise can be spatially correlated and spectrally varying. One-shot and unsupervised approaches, such as Unsupervised Hyperspectral Resolution Enhancement and Denoising (UHRED), reduce the need for paired high-SNR ground-truth data by learning from the structure of a single hyperspectral SRS dataset.[59] More recently, self-supervised methods such as Self-supervised PErmutation Noise2noise Denoising (SPEND) have been developed to remove non-independent noise from hyperspectral image stacks, using internal spatial-spectral redundancy rather than externally acquired clean references (Fig. 2 (b)).[60] Such approaches are particularly important for live-cell, metabolic, or high-dimensional chemical imaging, where repeated averaging may introduce motion artifacts or disturb biological processes.[84] Nevertheless, spatial–spectral redundancy does not by itself guarantee molecular fidelity, and reconstructed contrast should be validated against independent measurements or physically grounded spectral constraints whenever possible.

Although hardware noise suppression and computational denoising are discussed within the same technical family, they should not be regarded as physically equivalent. Hardware strategies improve the fidelity of the optical measurement itself, whereas computational methods operate on information already recorded by the detector. Denoising can improve apparent signal-to-noise ratio and image interpretability when weak but meaningful contrast is present, but it cannot reliably recover molecular information that is entirely absent below the physical measurement floor without relying strongly on prior assumptions. Excessive restoration may also introduce artificial structures or false-positive contrast. Computationally enhanced SRS should therefore be evaluated not only by visual image quality, but also by spectral fidelity, generalization across imaging conditions, uncertainty, and agreement with independent measurements. Within this review, computational methods used primarily for denoising are included in signal enhancement, whereas methods that additionally

recover spatial-frequency information, unmix molecular components, or infer biological states are discussed across the corresponding light-field- or information-enhancement sections. Hybrid platforms such as ultrasensitive reweighted visible SRS (URV-SRS) illustrate this increasing integration of optical detection and computational restoration.[63] Thus, modern SRS signal enhancement is increasingly a hardware–software co-design problem, in which optical noise suppression and computational restoration jointly define the usable sensitivity of the microscope.

3.2. *Resonance, excitation-wavelength, and plasmonic local-field enhancement*

A second technical family enhances SRS contrast by modifying the molecular response, excitation conditions, or local electromagnetic environment at the signal-generation stage. These approaches do not share a single physical mechanism, but they all seek to strengthen the Raman interaction or improve the effective detectability of the generated vibrational response before conventional SRL or SRG detection. Electronic pre-resonance and resonance enhance the molecular response through vibronic coupling, whereas Raman-probe design provides chromophores and vibrational tags optimized for these excitation conditions. Excitation-wavelength engineering can additionally alter Raman-response strength, spatial resolution, accessible spatial-frequency support, and detector performance. Plasmonic nanostructures follow a distinct route by confining and enhancing the local electromagnetic field around analyte molecules. These strategies are discussed together as signal-generation-oriented enhancement approaches, while their different physical origins, sample requirements, and biological constraints are considered separately.

Electronic pre-resonance SRS (EPR-SRS) enhances the vibrational response of chromophore-coupled Raman probes by tuning the excitation wavelength close to, but not fully resonant with, the electronic absorption band of the probe molecule. This pre-resonance condition strengthens vibronic coupling and substantially increases the effective Raman response and scattering cross-section of the designed probe while preserving the narrow vibrational linewidth that distinguishes Raman-based imaging from fluorescence.[61,65] As demonstrated in super-multiplex vibrational imaging, EPR-SRS enabled submicromolar detection of Raman-active dyes in living cells and supported a palette of spectrally narrow vibrational colors in the cell-silent window (Fig. 2(c)).[22] By coupling triple-bond vibrations to electronic transitions, designed EPR-SRS probes combine high sensitivity, spectral separability, and multiplexing capacity, making them useful for imaging organelles, biomolecular labels, and spatially resolved cellular composition beyond the color capacity of conventional fluorescence microscopy.[85,86] However, because this enhancement relies on designed chromophoric probes, EPR-SRS is most powerful for probe-based imaging and is not universally applicable to all endogenous biomolecules.

More recently, resonance enhancement has been pushed closer to the electronic absorption maximum. Electronic resonance SRS (ER-SRS) uses pump wavelengths rigorously resonant with electronic transitions and therefore can, in principle, provide even stronger signal amplification than pre-resonance excitation.[87] A recent demonstration of far-field single-molecule ER-SRS combined nonfluorescent Raman-amplified probes with independently tunable double optical parametric oscillators to optimize the signal-to-background ratio and detect single particles in solution and single molecules embedded in a polymer matrix.[88] Importantly, this sensitivity was achieved using specially engineered Raman-amplified probes with exceptionally large effective Raman responses under carefully optimized resonance conditions. It should therefore not be directly generalized to routine single-molecule detection of endogenous lipids, proteins, metabolites, or conventional small-molecule drugs. ER-SRS nevertheless demonstrates the potential of electronic resonance for fluorescence-free single-molecule vibrational detection, although electronic background, probe design, spectral tuning, and photostability remain important practical constraints.

Excitation-wavelength engineering, particularly the use of visible excitation, represents a related but mechanistically distinct strategy. Moving to shorter wavelengths can improve diffraction-limited spatial resolution and may increase effective SRS detectability through wavelength-dependent Raman interaction strength, proximity to electronic

pre-resonance, optical-transfer characteristics, and detector responsivity.[62] These effects should not be regarded as a universal enhancement produced by wavelength alone, because their relative contributions depend on the molecular target, laser configuration, detection system, and sample. However, visible excitation also increases the risk of photodamage, nonlinear background, and photothermal effects, particularly in live biological specimens. Therefore, visible SRS requires careful pulse-duration, wavelength, and power management. Recent work using frequency doubling of picosecond pulses demonstrated a widely tunable visible SRS platform capable of rapid multichannel imaging across different bond regions, showing how visible excitation can be implemented without relying entirely on femtosecond spectral focusing.[64]

A more integrated example is URV-SRS, which combines visible-wavelength excitation, extensive pulse chirping, ultrasensitive detection, self-supervised denoising, and Fourier-domain reweighting. In this strategy, visible excitation broadens the spatial-frequency support of the optical transfer function, while pulse chirping reduces peak power and helps suppress photodamage and non-Raman background. The self-supervised denoising step improves the detectability of weak metabolic signals, and Fourier reweighting amplifies high spatial-frequency components that are otherwise buried in noise. As a result, URV-SRS enabled label-free nanoscopy of intracellular metabolites with substantially improved sensitivity and sub-100-nm lateral resolution (Fig. 2(d)).[63] This example illustrates how excitation-wavelength engineering is increasingly becoming a system-level co-design problem, rather than a simple change of excitation color.

Beyond molecular resonance and excitation-wavelength engineering, plasmonic nanostructures can enhance SRS through localized electromagnetic-field confinement. Plasmon-enhanced SRS (PESRS) uses localized surface plasmon resonances in metallic nanostructures to strengthen the excitation field and nonlinear Raman interaction experienced by molecules within nanoscale hot spots. We use the term "plasmonic local-field enhancement" rather than the broader expression "near-field enhancement" to distinguish this mechanism from probe-based near-field microscopies such as tip-enhanced Raman spectroscopy or scattering-type near-field optical microscopy. In a representative study, plasmonic local-field enhancement enabled single-molecule detection using picojoule-level excitation, background subtraction, and denoising. Single-molecule behavior was supported by measurements of adenine isotopologues and statistical signatures including digital blinking and photobleaching, and the method was further applied to map adenine released from bacteria under starvation stress.[66] This single-molecule regime, however, depended on highly localized plasmonic hot spots, surface-associated analytes, carefully controlled backgrounds, and statistical validation. It therefore represents an ultrasensitive surface-enhanced sensing configuration rather than a general method for imaging freely distributed endogenous molecules at the single-molecule level. PESRS also remains closer to surface-enhanced chemical mapping than to routine imaging of intact cells or tissues. Its dependence on engineered nanostructures, nanoscale field heterogeneity, background subtraction, and potentially dispersive spectral line shapes limits spatial uniformity, quantitative reproducibility, biological compatibility, and general biomedical applicability.[67,89] PESRS is therefore best regarded as an ultrasensitive and spatially localized chemical-sensing approach rather than a mature general-purpose SRS imaging modality.

Overall, resonance, excitation-wavelength, and plasmonic local-field enhancement strengthen SRS contrast through different forms of signal-generation engineering. EPR-SRS and ER-SRS increase the response of specially designed probes through electronic coupling; visible excitation modifies spatial resolution, accessible spatial-frequency support, and, in selected cases, resonance conditions and effective signal strength; and PESRS confines electromagnetic fields within nanoscale plasmonic hot spots. These approaches extend SRS toward low-abundance probes, nanoscale structures, and proof-of-principle single-molecule detection, but their performance remains strongly dependent on probe design, excitation wavelength, electronic background, phototoxicity, local-field uniformity, and sample geometry. They should therefore be regarded as complementary and application-specific extensions of conventional nonresonant near-infrared SRS rather than universally applicable sensitivity gains.

3.3. *Stimulated Raman photothermal microscopy as an alternative vibrational readout*

SRP microscopy (also termed photothermal SRS, PT-SRS) provides a distinct route to signal enhancement by changing how Raman-resonant energy deposition is detected. Conventional SRS measures the minute SRL or SRG modulation carried by the pump or Stokes beam. In SRP, nonradiative relaxation of vibrationally excited molecules produces transient local heating, which generates a thermo-optic perturbation, such as a change in refractive index or scattering. A separate probe beam detects this secondary optical response. SRP is therefore more appropriately regarded as an alternative vibrational readout pathway than as a direct amplification of conventional SRL or SRG. (Fig. 2(e)).[68,69] Under suitable conditions, converting vibrational excitation into a photothermal response can produce a larger effective modulation depth and reduce the impact of laser intensity noise on weak-signal detection. SRP has been demonstrated in diverse biological samples, including viral particles, cells, and tissues, and may also facilitate compact or lower-cost implementations when direct SRS detection is limited by laser noise.[70] These characteristics make SRP a complementary approach to conventional SRS, particularly for weak targets or imaging systems in which direct detection of small intensity modulation is technically challenging.

However, SRP introduces trade-offs that differ from those of conventional SRS. The detected signal depends on Raman-resonant energy deposition, thermal diffusion, modulation frequency, probe-beam geometry, and the local thermo-optic properties of the sample, which can complicate quantitative interpretation in heterogeneous specimens.[90] Background absorption and cumulative sample heating also require careful control, particularly in live cells or temperature-sensitive biological systems. Moreover, because thermal diffusion and probe-beam scattering can generate nonlocal contributions from outside the nominal focal volume, the effective axial response may be broadened, weakening optical sectioning and depth-localization accuracy, especially in thick or strongly scattering samples. Thermal relaxation may additionally constrain the usable modulation frequency and imaging speed.

Overall, SRP expands weak-signal detectability by replacing the direct measurement of minute SRL or SRG modulation with a thermally mediated secondary optical readout. Its advantages are most relevant when conventional SRS is limited by laser intensity noise or insufficient modulation depth, but they must be balanced against thermal transport, background absorption, sample heating, spatial localization, and quantitative calibration. Future development will require optimized modulation and probe-beam geometries, improved optical–thermal modeling, and calibration strategies that relate photothermal contrast to molecular concentration while preserving biologically compatible illumination and spatial resolution.

3.4. *Quantum and emerging photonic enhancement*

Quantum-enhanced detection and emerging photonic field-enhancement technologies represent forward-looking routes that extend SRS beyond conventional classical free-space architectures. These approaches operate through distinct physical mechanisms and are grouped here because they share the broader character of emerging photonic technologies. Quantum-enhanced SRS uses nonclassical optical states to reduce measurement fluctuations below the classical shot-noise benchmark, whereas nanophotonic, cavity, and waveguide approaches strengthen light–matter interactions through resonant field buildup, optical confinement, or extended interaction lengths.

In conventional shot-noise-limited SRS microscopy, improving the signal-to-noise ratio generally requires detecting more photons, but the photon flux tolerated by biological samples is constrained by photodamage, phototoxicity, and heating. Quantum-enhanced SRS addresses this photon-budget limitation by introducing nonclassical light states, such as squeezed light, whose intensity fluctuations can be reduced below the standard quantum limit in the detected quadrature.[91,92] By lowering the measurement noise floor without increasing illumination dose, quantum correlations provide a route to improving SRS sensitivity under biologically constrained imaging conditions. A key demonstration of this concept used bright quantum-correlated illumination for quantum-enhanced nonlinear microscopy, achieving coherent Raman

imaging of molecular bonds in cells with a signal-to-noise ratio exceeding that of a comparable classical measurement under photodamage-limited illumination (Fig. 2(f)).[71] This improvement arose from reduced quantum noise in the detected field rather than stronger sample illumination, establishing that quantum optical resources can be practically integrated into nonlinear vibrational microscopy for photon-efficient biological imaging.

The achievable quantum advantage should nevertheless be distinguished between ideal and practical conditions. In principle, stronger squeezing produces a progressively lower noise variance in the measured quadrature. In practice, the observable improvement is reduced by optical loss, detector inefficiency, imperfect mode matching, phase instability, finite squeezing, and propagation through high-numerical-aperture imaging optics. Loss is particularly important because it mixes vacuum fluctuations into the detected mode and degrades the nonclassical state. Consequently, experimentally realized gains are generally incremental rather than orders of magnitude, but they can remain valuable when the classical system already operates near the shot-noise limit and further increases in illumination are prevented by sample damage.

Subsequent quantum-enhanced SRS developments have focused on improving compatibility with the optical powers and acquisition speeds required for practical microscopy. Because early implementations were limited by the brightness and power handling of squeezed-light sources, high-power QESRS was developed to operate at power levels comparable to state-of-the-art classical SRS microscopes while maintaining sub-shot-noise performance.[72] More recently, bright squeezed beams have enabled quantum-enhanced multispectral imaging of biological samples and living cells, showing that quantum correlations can improve imaging speed or signal-to-noise ratio without increasing optical dose.[73] Despite these advances, quantum-enhanced SRS remains technically demanding: efficient generation of bright squeezed light, preservation of quantum correlations through high-numerical-aperture optics, optical loss management, mode matching, and compatibility with broadband or hyperspectral acquisition all remain challenging. Furthermore, the benefit of quantum illumination becomes meaningful primarily when classical technical noise has already been sufficiently suppressed and the corresponding system operates close to the shot-noise limit. Quantum-enhanced SRS should therefore be viewed as a promising route for photon-efficient imaging under dose-limited conditions, rather than as a universal replacement for balanced detection, modulation engineering, or computational denoising.

Emerging photonic field-enhancement strategies seek to amplify SRS signals by confining optical fields in nanostructures, microcavities, waveguides, or resonant photonic modes. Demonstrations such as cavity-enhanced SRS in semiconductor nanowires show that resonant field buildup and nanoscale optical confinement can strengthen stimulated Raman interactions and reduce effective Raman thresholds.[74,93] These results suggest potential opportunities for integrated Raman sensing and miniaturized SRS systems.[75] However, most cavity- or nanophotonic-enhanced SRS studies remain closer to spectroscopy, nanophotonic devices, or chemical sensing than to general-purpose biomedical microscopy. Their reliance on specific material platforms, engineered resonator geometries, strong spatial confinement, and direct analyte–structure coupling makes translation to heterogeneous, hydrated, three-dimensional biological specimens challenging. Therefore, photonic field-enhancement should currently be viewed as an emerging enabling technology rather than an established biological SRS imaging modality.

Overall, quantum-enhanced and photonic enhancement strategies expand the conceptual boundary of SRS signal enhancement. Quantum-enhanced SRS targets the noise floor of measurement itself, whereas photonic enhancement seeks to strengthen light–matter interaction through engineered optical confinement. Their grouping reflects a shared technological frontier rather than a common physical mechanism. Both directions are likely to become more important as SRS microscopy moves toward lower light dose, weaker molecular targets, and more compact or integrated systems. Their future impact will depend on whether they can be combined with robust imaging workflows, broadband spectral access, biological compatibility, and quantitative calibration.

4. Acquisition Enhancement: Improving Chemical Information Throughput and Accessibility

Acquisition enhancement focuses on improving how efficiently SRS microscopy collects reliable chemical

information. In conventional SRS imaging, acquisition performance is constrained by coupled trade-offs among imaging speed, signal-to-noise ratio, spectral coverage, field of view, light dose, and system stability. Fast single- or few-frequency SRS can capture selected vibrational bands with high temporal resolution, but provides limited chemical information. Hyperspectral or broadband SRS can reveal richer molecular composition, but often requires wavelength scanning, delay scanning, multiplex detection, or more demanding data processing. Accordingly, the central goal of acquisition enhancement is not simply to maximize frame rate, but to increase the amount of reliable chemical and spectral information obtained per unit time while maintaining acceptable signal quality, light dose, and operational robustness.

To provide a consistent organizational logic, we arrange acquisition strategies primarily according to the spectral dimensionality obtained within each measurement cycle, while retaining their enabling hardware and computational technologies as secondary descriptors. High-speed single- and few-frequency acquisition, supported by rapid scanning and robust laser platforms, prioritizes temporal resolution, stability, and practical usability for dynamic imaging, high-throughput screening, and clinical workflows.[15,94] Simultaneous or quasi-simultaneous multichannel acquisition uses multiplex, multicolor, or scanning-free schemes to collect several discrete Raman contrasts with reduced temporal overhead. Continuous or rapidly encoded hyperspectral and broadband acquisition expands spectral coverage through spectral focusing, rapid delay scanning, time encoding, or Fourier-domain detection.[14,16,95,96] Finally, sparse, compressed, and computational acquisition reduces the number of physical measurements required to reconstruct high-dimensional spatial–spectral data.[26,97,98] This progression from selected bands to multiple discrete channels, continuous spectral coverage, and computationally reconstructed measurements provides the organizational framework for this section (Fig. 3). Representative performance metrics include reliable chemical-information throughput, frame rate or pixel dwell time, spectral acquisition time, spectral dimensionality per measurement cycle, sampling ratio or acceleration factor, and long-term system stability.

4.1. *High-speed single- and few-frequency acquisition enabled by robust SRS platforms*

High-speed single- and few-frequency acquisition is particularly effective when a biological or clinical task can be addressed using one or a small number of predefined Raman shifts. In point-scanning SRS microscopy, the imaging rate is jointly determined by pixel dwell time, scanning hardware, modulation frequency, detector bandwidth, and the signal-to-noise ratio required for reliable contrast. Shortening the pixel dwell time can increase the frame rate, but it also reduces the number of detected photons and may compromise image quality. Therefore, high-speed SRS acquisition requires coordinated optimization of scanning speed, laser stability, modulation strategy, detection bandwidth, and light dose.

Early fast SRS imaging mainly relied on high-frequency modulation, lock-in detection, and rapid beam scanning to record selected Raman bands at video-rate or near-video-rate speeds.[3,53] This strategy is effective when only a few predefined vibrational contrasts are needed, such as lipid mapping, isotope tracing, or monitoring cellular dynamics. However, broader biological and clinical applications require more than frame-rate improvement. Long-term stability, operational simplicity, wavelength tunability, and robustness against environmental perturbations are equally important for making SRS microscopy usable outside specialized optical laboratories.[99]

Robust laser platforms are therefore considered here as enabling infrastructure for sustained high-speed selected-band acquisition. Conventional SRS systems often rely on synchronized solid-state ultrafast lasers or optical parametric oscillators that provide high-quality pulses but are bulky, costly, and environmentally sensitive. Fiber-laser-based SRS platforms address these limitations by offering more compact, alignment-tolerant, and stable dual-wavelength excitation while maintaining shot-noise-limited sensitivity and high-quality chemical imaging.[15] Their translational impact is particularly evident in stimulated Raman histology (SRH), where portable fiber-laser SRS microscopes enable rapid imaging of fresh, unprocessed surgical specimens and generate virtual histology images without conventional freezing, sectioning, or staining (Fig. 3 (a)).[100] In this context, acquisition enhancement extends beyond frame-rate improvement to include

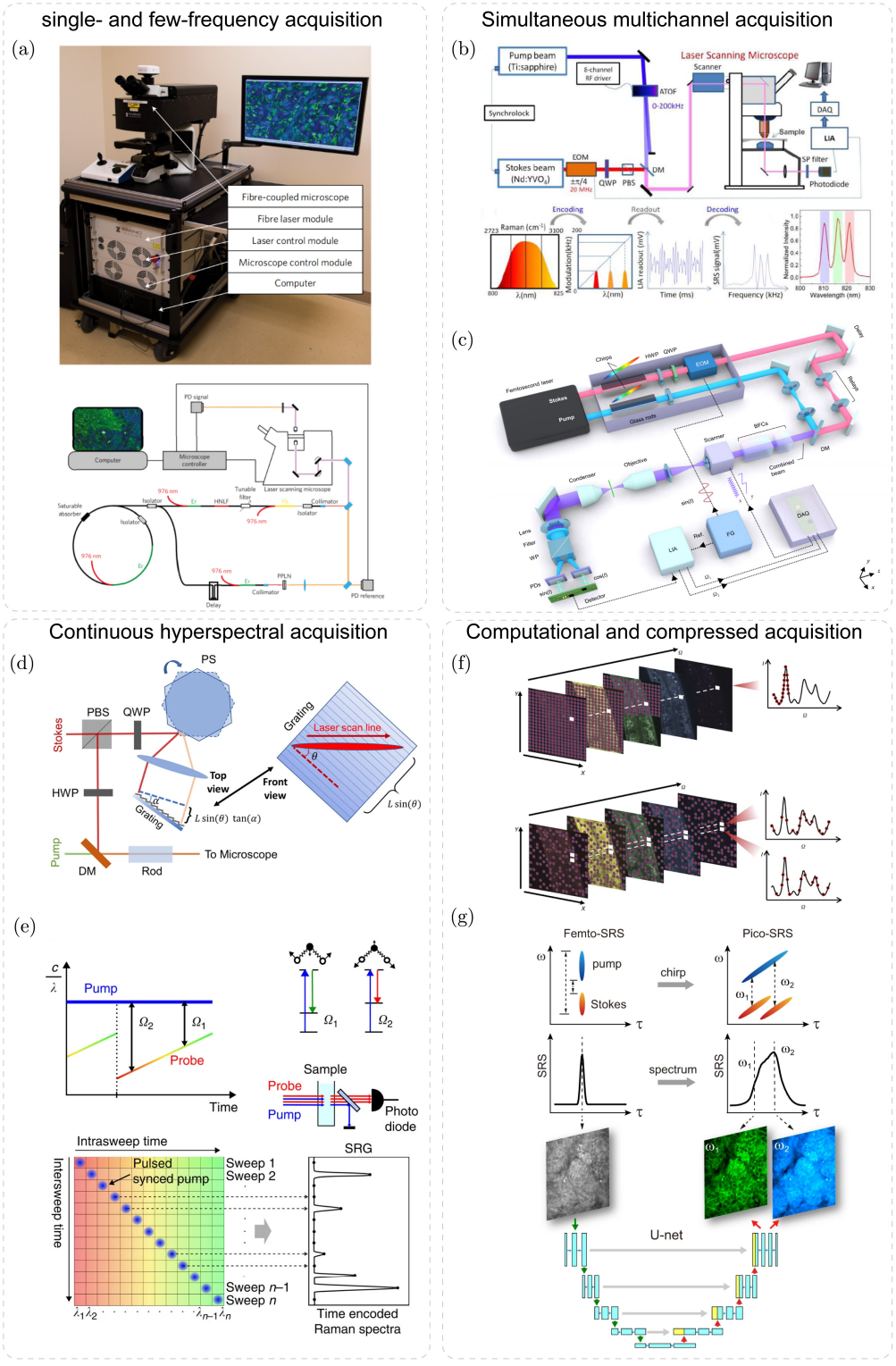

Fig. 3. Representative acquisition-enhancement strategies organized according to spectral acquisition dimensionality. (a) High-speed single- and few-frequency acquisition using a robust fiber-laser SRS platform. Adapted with permission from Ref. 100. (b) and (c) Simultaneous multichannel acquisition through modulation multiplexing and scanning-free dual-Raman-shift detection. Reproduced with permission from Refs. 4 and 105, respectively. (d) and (e) Continuous or rapidly encoded hyperspectral acquisition through polygon-scanner-based delay tuning and time encoding. Reproduced with permission from Refs. 107 and 16, respectively. (f) and (g) Computational or compressed acquisition through sparse sampling with matrix completion and deep-learning reconstruction from single-shot femtosecond SRS. Reproduced with permission from Refs. 26 and 98, respectively.

simplified sample preparation, workflow compatibility, system reproducibility, and large-scale clinical data collection, making SRH a representative example of how robust SRS platforms can support translational imaging and downstream computational diagnosis.[94]

Fiber-laser platforms can also improve spectral accessibility when combined with rapid and wide wavelength tuning. Rapidly tunable fiber-laser SRS systems have demonstrated multi-window imaging across biologically important Raman regions, including the fingerprint, C–D, and C–H bands.[54] Frame-to-frame wavelength-tunable fiber sources further allow multicolor SRS acquisition from the fingerprint to the C–H stretching region within millisecond-scale wavelength steps, avoiding the slow mechanical tuning often associated with solid-state OPO systems.[99] Self-synchronized two-color fiber lasers can also simplify pump–Stokes synchronization and reduce timing jitter, which is beneficial for fast coherent Raman imaging.[101] These methods are included in this section because they provide rapid sequential access to a limited set of predefined Raman bands; simultaneous multichannel and continuous hyperspectral acquisition are discussed separately in Secs. 4.2 and 4.3.

Overall, high-speed single- and few-frequency SRS provides high temporal efficiency when targeted chemical contrasts are sufficient. Its practical performance depends on balancing frame rate, signal-to-noise ratio, light dose, long-term stability, and wavelength-switching speed. Robust laser platforms improve accessibility and reproducibility, whereas rapid wavelength tuning expands targeted chemical coverage but introduces additional requirements for calibration and synchronization. When several chemical contrasts must be acquired within the same dynamic event, simultaneous or quasi-simultaneous multichannel strategies become necessary, as discussed in the following section.

4.2. *Simultaneous and quasi-simultaneous multichannel acquisition: Multiplex, multicolor, and scanning-free SRS acquisition*

Simultaneous and quasi-simultaneous multichannel acquisition reduces the temporal cost of chemical specificity when several predefined Raman contrasts are required within the same biological or clinical measurement. Unlike single- and few-frequency acquisition, which usually accesses selected Raman bands sequentially, multichannel approaches encode two or more discrete chemical contrasts in wavelength, modulation frequency, phase, polarization, or detection channels and recover them within the same or closely synchronized imaging cycle. This parallelization increases chemical-information throughput, improves temporal co-registration, and reduces motion-induced mismatch in live cells, fresh tissues, and other dynamic specimens. Here, multichannel acquisition refers primarily to a limited number of discrete Raman contrasts; continuous or densely sampled spectral acquisition is discussed separately in Sec. 4.3.

Early multicolor SRS approaches used spectral shaping and multichannel detection to overcome the single-band limitation of conventional picosecond SRS. In one implementation, a grating-based pulse shaper generated spectrally tailored excitation, while a grating-based spectrograph enabled simultaneous detection of multiple SRS channels.[25] This design allowed selected vibrational bands, such as CH_2 and CH_3 stretching modes, to be measured in parallel and used for simultaneous mapping of lipid- and protein-rich regions. These approaches established the basic idea that acquisition speed and chemical specificity can be improved by reducing the need for slow sequential spectral scanning.

Another important route is modulation multiplexing. Instead of separating Raman channels only by wavelength or time, different spectral components or excitation channels can be modulated at distinct radio frequencies and recovered by Fourier or lock-in demodulation (Fig. 3(b)).[4,102] This allows multiple molecular species to be detected in real time from a single acquisition stream. The strength of modulation multiplexing is that it encodes chemical information into the modulation domain, enabling simultaneous readout without sacrificing the chemical selectivity of SRS. Its practical implementation, however, requires careful control of modulation depth, channel crosstalk, detector bandwidth, and demodulation accuracy.

For tissue imaging and digital pathology, two-color SRS is particularly valuable because many histological contrasts can be approximated by relative protein- and lipid-associated Raman signals.[103] Dual-phase SRS enables real-time two-color imaging by assigning two Stokes beams to orthogonal modulation phases and recovering the two

Raman channels from the in-phase and quadrature outputs of a phase-sensitive lock-in amplifier, allowing lipid- and protein-associated contrasts to be acquired simultaneously at the speed of single-color SRS.[104] More recent scanning-free dual-Raman-shift SRS further simplifies this idea by using birefringent crystals to introduce controlled optical path differences and orthogonal polarization states, thereby encoding paired contrasts such as CH_3 and CH_2 into synchronized detection channels without spectral scanning (Fig. 3(c)).[105] These strategies improve temporal registration, reduce motion artifacts, and are useful for dynamic biomolecular imaging, lipid-droplet analysis, rapid tissue assessment, and label-free digital histology. Although collinear balanced detection can improve signal-to-noise ratio in such systems, their primary contribution lies in simultaneous dual-channel acquisition and higher chemical information throughput rather than single-channel signal amplification.

Overall, multiplex, multicolor, and scanning-free SRS methods enhance acquisition by moving chemical contrast from a sequential measurement problem toward a parallel encoding and detection problem. Their main advantages are reduced motion artifacts, improved temporal co-registration, higher information throughput, and better suitability for dynamic or clinical samples. At the same time, these methods introduce new constraints, including channel crosstalk, calibration complexity, modulation bandwidth, and the limited number of channels that can be robustly separated in real time. Future development will likely combine optical multiplexing, polarization or phase encoding, balanced detection, and computational demultiplexing to achieve faster and more scalable multichannel SRS imaging. When continuous or densely sampled vibrational spectra are required rather than a limited set of discrete contrasts, hyperspectral and broadband acquisition strategies become necessary, as discussed in the following section.

4.3. *Continuous and rapidly encoded hyperspectral and broadband SRS acquisition*

Hyperspectral and broadband SRS acquisition extends chemical-information throughput from a limited number of discrete Raman channels to continuous or densely sampled vibrational spectra. Compared with single-frequency SRS, hyperspectral SRS records image stacks over multiple Raman shifts and enables spectral unmixing, quantitative chemical mapping, and identification of overlapping molecular components. However, acquiring the spectral dimension usually requires wavelength scanning, delay scanning, multiplex detection, or broadband excitation, which can increase acquisition time, system complexity, and photodose. The central challenge is therefore to increase spectral information per unit time while maintaining spectral fidelity, sensitivity, and image quality.

Spectral focusing has become a major strategy for fast hyperspectral SRS. By temporally chirping femtosecond pump and Stokes pulses, the instantaneous frequency difference is mapped onto the pump–Stokes delay, allowing Raman shifts to be tuned by scanning the delay. This approach greatly accelerates hyperspectral SRS while retaining the image quality of narrowband SRS, and has been widely used for biological imaging in the C–H stretching region. To overcome the speed limit of mechanical delay scanning, rapid scanning optical delay lines, acousto-optic delay lines, and polygon-scanner-based delay tuning have been developed (Fig. 3(d)).[50,96,106,107] In particular, polygon-scanner fingerprint SRS enabled microsecond-scale spectral acquisition in the fingerprint region, extending high-speed spectroscopic SRS toward more chemically specific molecular signatures.

Broadband and time-encoded SRS provide another route to accelerate spectral acquisition by encoding Raman information into wavelength, time, or interferometric domains rather than measuring Raman shifts sequentially. Time-encoded Raman uses rapidly swept laser sources to map vibrational information onto the time axis, offering broad spectral coverage and high spectral resolution in a fiber-based format (Fig. 3(e)).[16] Fourier-transform and other interferometric SRS schemes similarly recover broadband vibrational spectra through temporal or frequency-domain encoding.[108] More recently, simultaneous dual-band hyperspectral SRS has enabled image stacks from two independently selected Raman windows, allowing joint access to regions such as the fingerprint, C–D, and C–H bands within one system.[109]

Overall, hyperspectral and broadband acquisition transforms SRS from selected-band imaging into spectroscopic molecular imaging. Spectral

focusing, rapid delay scanning, polygon-scanner tuning, time encoding, Fourier-domain detection, and dual-band acquisition all address the same core question: how to obtain more reliable spectral information per unit time. The remaining trade-offs include spectral resolution, spectral range, sensitivity, calibration stability, system complexity, and data-processing burden. When exhaustive or densely sampled hyperspectral acquisition remains impractical, sparse, compressed, and computational strategies can further reduce the number of physical measurements required, as discussed in Sec. 4.4.

4.4. *Sparse, compressed, and computational acquisition*

When exhaustive spatial–spectral sampling is impractical, sparse, compressed, and computational acquisition can improve the efficiency of SRS imaging by reducing the number of measurements needed to reconstruct chemically informative images. Unlike post-acquisition denoising applied to conventionally sampled data, these approaches deliberately select, encode, or omit measurements during acquisition and then use spatial continuity, spectral sparsity, low-rank structure, or learned relationships for reconstruction. Computation therefore becomes part of the measurement design itself, with the goal of reducing acquisition time, photodose, and data burden while preserving chemically relevant information.

Sparse spectroscopic SRS is a representative example. Instead of measuring every pixel across a full hyperspectral image stack, three-dimensional sparsely sampled spectroscopic SRS acquires only a subset of the spatial–spectral volume and reconstructs the full dataset through matrix completion (Fig. 3(f)).[26] Similarly, multi-window sparse spectral sampling selects a limited number of informative Raman frequencies across the fingerprint, cell-silent, and high-wavenumber regions, allowing targeted chemical imaging without densely scanning the entire spectrum.[110] These strategies are especially useful when dynamic biological processes or large fields of view make full hyperspectral acquisition impractical.

Compressed optical encoding and deep-learning-based acquisition further extend this concept. Spatial light-modulated SRS tailors broadband excitation with sparse-sampling masks, encoding selected spectral features before detection for rapid multiplexed vibrational imaging.[97] Deep-learned single-shot femtosecond SRS histology uses a neural network to convert fast but spectrally mixed femtosecond SRS images into chemically resolved picosecond-like SRS contrasts, preserving imaging speed while recovering chemical specificity (Fig. 3(g)).[98] In these cases, computation does not merely analyze SRS images after acquisition; it becomes part of the acquisition strategy itself.[111]

Overall, sparse, compressed, and computational acquisition replaces exhaustive measurement with selective sampling, optical encoding, and model-based reconstruction. Its performance should therefore be evaluated not only by frame rate, but also by sampling ratio, acceleration factor, reconstruction error, spectral fidelity, photodose, calibration stability, and generalization across heterogeneous samples. The achievable efficiency depends on whether the assumed sparsity, low-rank structure, or learned relationship remains valid for the specimen under study. These approaches complete the acquisition hierarchy developed in this section by showing that chemical-information throughput can be increased not only by faster or more parallel hardware, but also by measuring fewer, more informative data points.

5. Light-field Enhancement: Excitation-, Propagation-, and Collection-side Strategies for Depth, Resolution, and Volumetric Imaging

Light-field enhancement addresses how optical fields are delivered, shaped, propagated, exploited, and collected throughout the SRS imaging pathway to improve penetration depth, spatial and axial resolution, and volumetric access. In this paper, the term is used in a broad operational sense rather than as a synonym for direct excitation-field engineering. It therefore encompasses excitation-field and wavefront control, propagation and spatial encoding, nonlinear spatial-response manipulation, and detection geometries that exploit the redistribution of signal-carrying photons in thick or scattering specimens. Although these approaches act through distinct physical mechanisms, they share the goal of overcoming limitations in depth of field, scattering-induced attenuation, wavefront aberration, and signal collection. These issues are

particularly important in thick tissues, organoids, and other three-dimensional biological specimens, where conventional Gaussian-focus point scanning provides limited access to deep and volumetric molecular information.

Recent light-field-enhanced SRS methods can be grouped into three directions. First, Bessel-beam projection and tomographic SRS use extended-depth excitation, projection imaging, angular reconstruction, phase modulation, or time-of-flight encoding to achieve rapid volumetric chemical imaging.[27,112–115] Second, super-resolution SRS manipulates nonlinear vibrational responses, photoswitchable Raman probes, or interferometric excitation fields to overcome the diffraction-limited resolution of conventional SRS.[18,28,116–119] Third, wavefront engineering, adaptive optics, and scattering-tolerant detection improve SRS performance in optically heterogeneous or turbid samples by correcting aberrations, controlling focal fields, or optimizing signal collection.[120–123] Together, these strategies extend SRS microscopy from thin-sample chemical imaging toward deep, three-dimensional, and nanoscale molecular imaging (Fig. 4). Representative performance metrics include penetration depth, lateral and axial resolution, depth of field, optical sectioning, volumetric imaging efficiency, and robustness to scattering and aberration.

5.1. *Bessel-beam projection, tomography, and depth-resolved volumetric SRS*

One major route for light-field enhancement in SRS microscopy is to extend the excitation field along the axial direction and use the resulting projection or depth-encoded signal for volumetric chemical imaging. Conventional Gaussian-focus SRS provides optical sectioning but usually requires point-by-point and plane-by-plane scanning to build a three-dimensional image stack. This process can be slow for thick or dynamic specimens. Bessel beams, with their elongated focal region and quasi-non-diffracting propagation, offer an alternative excitation geometry that allows a three-dimensional volume to be interrogated through two-dimensional lateral scanning.

Bessel-beam-based stimulated Raman projection microscopy introduced extended-depth excitation into volumetric SRS imaging. By replacing the conventional Gaussian focus with a Bessel-like excitation field, SRS signals can be integrated over an elongated axial range, allowing three-dimensional chemical content to be captured as a two-dimensional projection image without mechanical z-scanning. This projection strategy improves volumetric imaging speed and is useful when rapid volume-level chemical quantification is more important than resolving every axial plane independently. Because projection imaging compresses depth information, stimulated Raman projection tomography (SRPT) further combines Bessel-beam projection with tomographic reconstruction: projection images acquired from multiple viewing angles are used to recover the three-dimensional distribution of chemical components, linking light-field engineering with computational reconstruction (Fig. 4(a)).[27]

Subsequent developments have aimed to make SRS tomography faster and more practical. Sparse-view reconstruction-assisted SRPT reduces the number of angular projections needed for volumetric recovery, while tilt-angle SRPT uses tilted excitation beams to generate angle-dependent projections without physically rotating the sample.[112,113] These strategies are important for live cells, fragile specimens, or integrated microscopy platforms where sample rotation is difficult. More recent depth-resolved methods address the axial-localization limit of projection imaging more directly. Time-of-flight-resolved Bessel light bullet-enabled SRS introduces temporal depth encoding into the Bessel excitation geometry, allowing depth-resolved chemical information to be recovered without mechanical z-scanning (Fig. 4(b)).[115] Together, these methods show that volumetric SRS is moving from simple projection imaging toward a co-designed framework of excitation geometry, sampling strategy, temporal or angular encoding, and computational reconstruction.

Phase-modulated SRS tomography provides another route to rapid three-dimensional chemical imaging.[114] Instead of relying only on sample rotation or extended-depth projection, phase modulation encodes volumetric information into the excitation and detection process, allowing rapid label-free 3D chemical imaging of cells and tissues. Together with phase-controlled focusing and aberration-corrected SRS, these methods indicate that the future of volumetric SRS will likely combine engineered excitation fields, phase or temporal

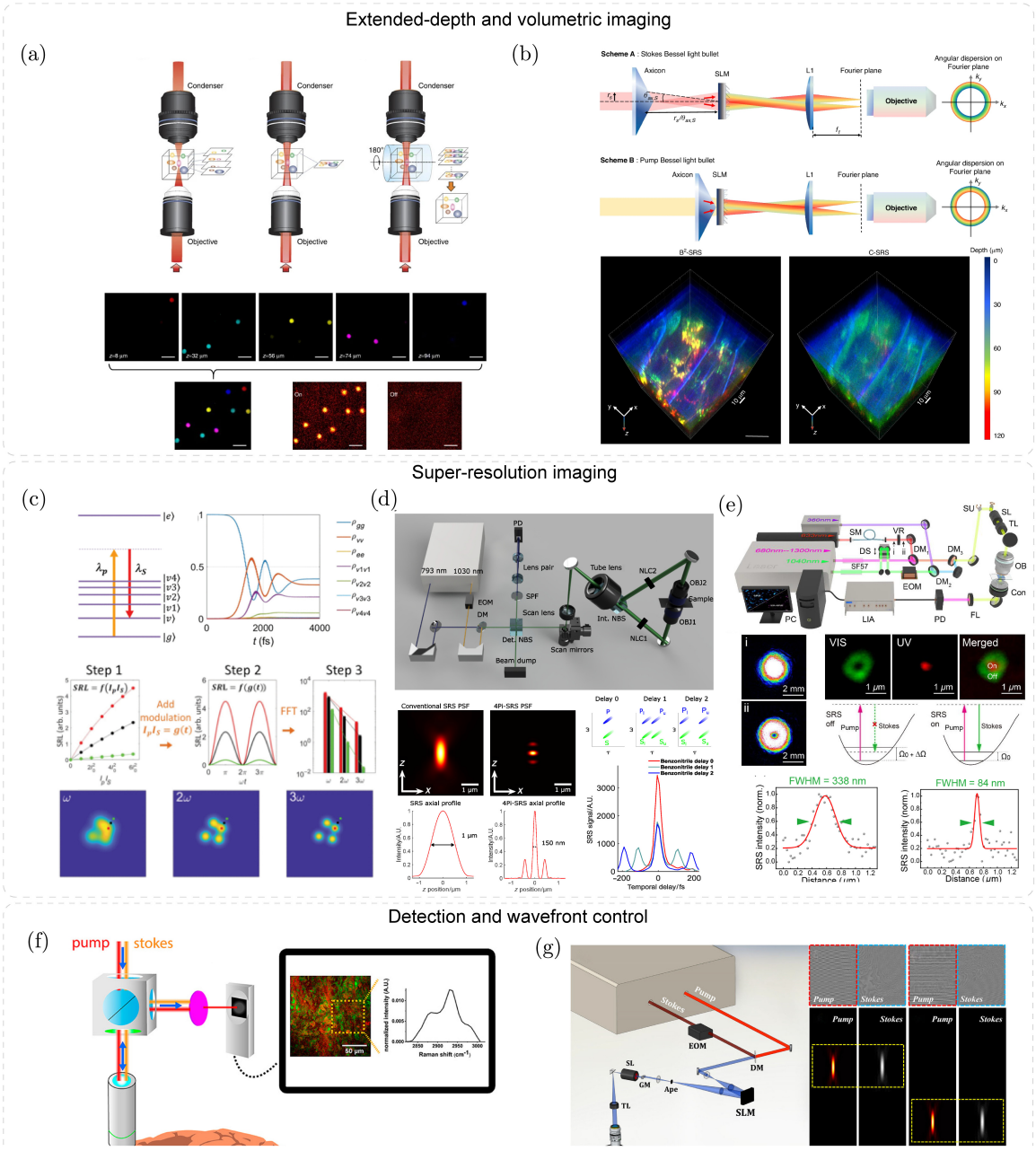

Fig. 4. Representative light-field-enhancement strategies organized by their dominant imaging functions. (a) and (b) Extended-depth and volumetric imaging through Bessel-beam projection tomography and Bessel light bullets. Adapted with permission from Refs. 27 and 115, respectively. (c)–(e) Super-resolution imaging through saturation-based modulation, 4Pi interference, and photoswitchable vibrational nanoscopy. Adapted with permission from Refs. 28, 116 and 119, respectively. (f) and (g) Detection and wavefront control through epi-detected SRS and adaptive optics for imaging in scattering specimens. Reproduced with permission from Refs. 120 and 123, respectively.

encoding, and computational reconstruction to improve depth, speed, and chemical specificity.[121]

In addition to optical-field engineering, sample-engineering strategies can also extend the depth range of SRS volumetric imaging. Tissue clearing does not directly reshape the excitation beam, but it reduces scattering and refractive-index heterogeneity, thereby improving light delivery and signal collection in thick specimens.[124] Clearing-enhanced SRS couples Raman-tailored tissue clearing with SRS microscopy and has demonstrated markedly increased imaging depth for volumetric chemical

imaging of tumor spheroids, brain tissues, and tumor xenografts based on endogenous protein and lipid contrast.[125–127] Therefore, tissue clearing should be viewed as a complementary depth-enhancement strategy that can work alongside Bessel beams, tomography, wavefront correction, and adaptive optics.

Overall, Bessel-beam projection, tomography, depth encoding, and clearing-assisted SRS expand SRS microscopy from two-dimensional chemical mapping toward volumetric molecular imaging. Their common goal is to reduce the cost of axial scanning and improve access to three-dimensional chemical information. The remaining challenges include projection artifacts, reconstruction fidelity, axial resolution, scattering-induced distortion, photodose management, and compatibility with live or clinically relevant specimens. Addressing these challenges will require continued integration of light-field design, sampling theory, tissue preparation, and computational reconstruction.

5.2. *Super-resolution SRS by optical-field and nonlinear response engineering*

Another important direction of light-field enhancement is super-resolution SRS, which aims to overcome the diffraction-limited spatial resolution of conventional far-field SRS microscopy. Because SRS contrast is generated through coherent nonlinear light–matter interaction, its effective spatial response can be modified not only by the excitation focus, but also by nonlinear vibrational saturation, structured illumination, interferometric field engineering, or photoswitchable Raman probes. These strategies extend SRS from subcellular chemical imaging toward nanoscale vibrational imaging.

Saturated stimulated Raman scattering (SSRS) provides a direct route to far-field super-resolution by exploiting the nonlinear saturation of the SRS response (Fig. 4(c)).[116] Under strong excitation, the SRS signal no longer increases linearly with optical intensity, and higher-order nonlinear components can be extracted to narrow the effective point-spread function. This allows SSRS to achieve vibrational imaging beyond the conventional diffraction limit without relying on fluorescence labels. However, saturation-based SRS typically requires high optical intensity, which may increase photodamage, local heating, and nonlinear background in biological specimens.

Structured light and spatial-frequency engineering provide another route to super-resolution SRS. Phase-shifted spatial frequency modulation SRS introduces patterned pump or Stokes excitation and recovers high spatial-frequency information through phase-shifted modulation and computational reconstruction.[117] Compared with saturation-based methods, this strategy enhances resolution by encoding otherwise inaccessible spatial frequencies into the detected SRS signal. Interferometric light-field engineering, represented by 4Pi-SRS, further improves spatial resolution by using counter-propagating excitation fields to narrow the axial point-spread function (Fig. 4(d)).[119] This is particularly valuable because conventional SRS usually has poorer axial than lateral resolution. The main challenges for these approaches are optical alignment, phase stability, modulation accuracy, and compatibility with live biological samples.[128]

Photoswitchable probes offer a probe-enabled route to super-resolution imaging.[129] Early switchable SRS microscopy introduced photochromic vibrational probes whose Raman frequency or SRS intensity can be reversibly controlled by light, enabling switchable vibrational contrast.[130] Building on this concept, reversible saturable optical Raman transitions (RESORT) microscopy uses reversible saturable optical Raman transitions and bright photoswitchable Raman probes to generate super-resolution SRS contrast under low-power control light (Fig. 4(e)).[28,118] Instead of relying solely on high-intensity vibrational saturation, this approach spatially controls the activation or depletion of Raman probes, making it especially attractive for small-molecule, organelle-targeted, or cell-silent-window imaging.[131]

Several adjacent strategies also contribute to the super-resolution SRS landscape but should be distinguished from optical-field and nonlinear-response engineering. A-PoD achieves super-resolved SRS images through adaptive pointillism deconvolution rather than by changing the excitation field or molecular response, so it is better discussed under information enhancement.[132] Expansion SRS physically enlarges the specimen before imaging and is therefore a sample-engineering strategy rather than a light-field strategy.[133] These methods are complementary to optical super-resolution SRS and

may be combined with it in future nanoscale chemical imaging workflows.

Overall, super-resolution SRS can be achieved through nonlinear saturation, structured illumination, interferometric focal-field engineering, photoswitchable Raman probes, computational deconvolution, or sample expansion. These approaches differ in optical power requirement, labeling strategy, system complexity, spatial resolution gain, and biological compatibility. Future developments will likely combine low-phototoxicity Raman probes, advanced light-field control, low-noise detection, and computational reconstruction to achieve nanoscale chemical imaging with improved specificity and reduced sample perturbation.

5.3. *Wavefront control and detection geometry for SRS imaging in scattering specimens*

For thick tissues and optically heterogeneous specimens, light-field enhancement must address not only focal-field design, but also scattering, aberration, and signal collection. Conventional forward-detected SRS performs well in thin or transparent samples because the SRL or gain is mainly carried by the transmitted pump or Stokes beam. In thick tissues, however, scattering attenuates the excitation beams, distorts the focal volume, and redirects part of the signal-carrying photons away from the forward direction. Improving SRS imaging in such specimens therefore requires complementary strategies acting at both the excitation and detection sides.

Epi-detected SRS is included here as a detection-side light-field strategy rather than as a direct excitation-field-engineering method. When conventional forward transmission detection is impractical, epi-detection exploits the scattering-mediated redistribution of signal-carrying photons toward the backward direction. Because SRS is primarily generated in the forward phase-matched direction, epi-SRS relies on tissue scattering to redirect part of the signal-carrying photons back to the excitation objective (Fig. 4(f)).[47,120] This makes epi-detection useful for thick tissue imaging, as demonstrated in epi-detected hyperspectral SRS for glioblastoma tissue subtyping and real-time two-color SRS imaging of thick brain tissue.[134] However, epi-SRS signal strength and image quality depend strongly on tissue scattering, collection efficiency, and imaging depth, so it should be viewed as a complementary detection strategy rather than a universal solution for deep SRS imaging.

Complementary excitation-side strategies use phase, wavefront, and adaptive-optics control to preserve focal quality and pump–Stokes overlap in heterogeneous specimens. Refractive-index mismatch and tissue-induced aberrations broaden the focal volume, reduce excitation overlap, and degrade SRS signal and resolution. Phase-controlled SRS addresses this problem by shaping the excitation wavefront and programming the focal-field position or phase structure, especially when combined with aberration correction for rapid volumetric deep-tissue imaging.[121] Adaptive optics further corrects specimen-induced aberrations by optimizing a deformable mirror or spatial light modulator according to feedback metrics such as SRS intensity or image contrast.[122] Because SRS depends on the joint spatial and temporal overlap of pump and Stokes beams, polychromatic adaptive optics is particularly important: it corrects wavelength-dependent aberrations affecting the two excitation colors and helps maintain co-focused beams in turbid, multicolor, or hyperspectral imaging (Fig. 4(g)).[123] Together, epi-detection, phase-controlled focusing, adaptive optics SRS (AO-SRS), and polychromatic adaptive optics SRS (PAO-SRS) form a scattering-tolerant toolkit for improving depth, contrast, and resolution in optically heterogeneous biological specimens.

Overall, epi-detection and wavefront correction provide complementary detection- and excitation-side routes for improving SRS imaging in optically heterogeneous specimens. Epi-detection improves access to thick samples when transmission detection is unavailable, while phase control and adaptive optics actively preserve focal quality and beam overlap in heterogeneous tissues. Their remaining challenges include limited collection efficiency, reliable feedback metrics, correction speed, optical loss, chromatic aberration, and robustness across diverse biological specimens. Future deep-tissue SRS will likely combine optimized detection geometry, wavefront correction, engineered excitation fields, sample clearing, and computational reconstruction to improve imaging depth without sacrificing chemical specificity or quantitative reliability.

6. Information Enhancement: Expanding Molecular Specificity and Multidimensional Readout

Information enhancement aims to expand what can be interpreted from SRS microscopy beyond the intensity of one or several Raman bands. Conventional SRS provides chemically specific contrast based on selected vibrational transitions, but many biological questions require more than simple molecular abundance maps.[135] In complex cells and tissues, Raman signals often arise from overlapping molecular species, heterogeneous biochemical states, anisotropic molecular organization, dynamic metabolic processes and spatial features that are not directly resolved in the raw intensity image. Therefore, information-enhanced SRS focuses on extracting richer molecular, structural, and functional information from the acquired vibrational data.

This direction differs from signal, acquisition, and light-field enhancement. Signal enhancement improves the detectability of weak vibrational contrast; acquisition enhancement increases the efficiency of data collection; light-field enhancement improves depth, resolution, and volumetric access. By contrast, information enhancement improves the interpretability and dimensionality of the SRS readout. It asks how SRS images can distinguish chemically similar species, quantify molecular mixtures, report biochemical states, reveal molecular orientation, recover hidden spatial information, or support diagnostic and biological decision-making. Accordingly, the methods in this section are organized primarily according to the type and level of information obtained, rather than according to the specific optical or computational technique used.

Recent advances in information-enhanced SRS can be grouped into four directions. First, spectral unmixing and computational molecular mapping use hyperspectral data and chemometric or machine-learning algorithms to resolve overlapping molecular components.[19,136–139] Second, functional and biochemical-state readout extends SRS from compositional imaging to molecular state imaging, including lipid order, metabolic activity, drug uptake, isotope incorporation, and protein secondary structure.[140–146] Third, polarization-, orientation-, and tensor-resolved SRS introduces additional physical dimensions beyond scalar intensity, enabling sensitivity to molecular alignment, anisotropy, and supramolecular organization.[147–151] Finally, computational reconstruction, virtual staining, and AI-assisted interpretation convert SRS or SRH images into higher-level information, including super-resolved spatial features, cellular phenotypes, and digital pathology outputs.[94,98,132,152–156] Together, these strategies transform SRS microscopy from bond-selective imaging into multidimensional molecular analysis (Fig. 5). Because the outputs vary across these subcategories, performance is evaluated using task-specific metrics, including component-separation fidelity, biochemical-state sensitivity, orientation or tensor accuracy, spatial-reconstruction fidelity, diagnostic or molecular-classification performance, and preservation of quantitative interpretability.

6.1. *Spectral to composition mapping*

Spectral unmixing is one of the most established routes for information enhancement in SRS microscopy. Although single-frequency SRS provides strong contrast at selected Raman shifts, biological samples usually contain multiple molecular species with overlapping vibrational bands. Hyperspectral SRS addresses this limitation by recording a vibrational spectrum at each pixel, but the resulting image stack must be computationally decomposed before it can be interpreted as molecular maps.

Classical chemometric methods laid the foundation for quantitative hyperspectral SRS analysis by decomposing overlapping Raman bands into component spectra and concentration maps. Early hyperspectral SRS studies used multivariate curve resolution, and related approaches such as nonnegative matrix factorization, principal component analysis, least-squares fitting, and multivariate curve resolution-alternating least squares (MCR-ALS) further enabled the separation of mixed biochemical signatures in cells and tissues.[19,157–159] When prior chemical information is available, reference-guided strategies provide more targeted molecular mapping. Penalized reference matching SRS (PRM-SRS) integrates hyperspectral SRS with reference-based spectral matching to identify multiple molecular species in complex biological samples, allowing chemically similar components to be distinguished more reliably than by unsupervised decomposition alone (Fig. 5(a)).[136] Together, these methods transform hyperspectral SRS from a stack

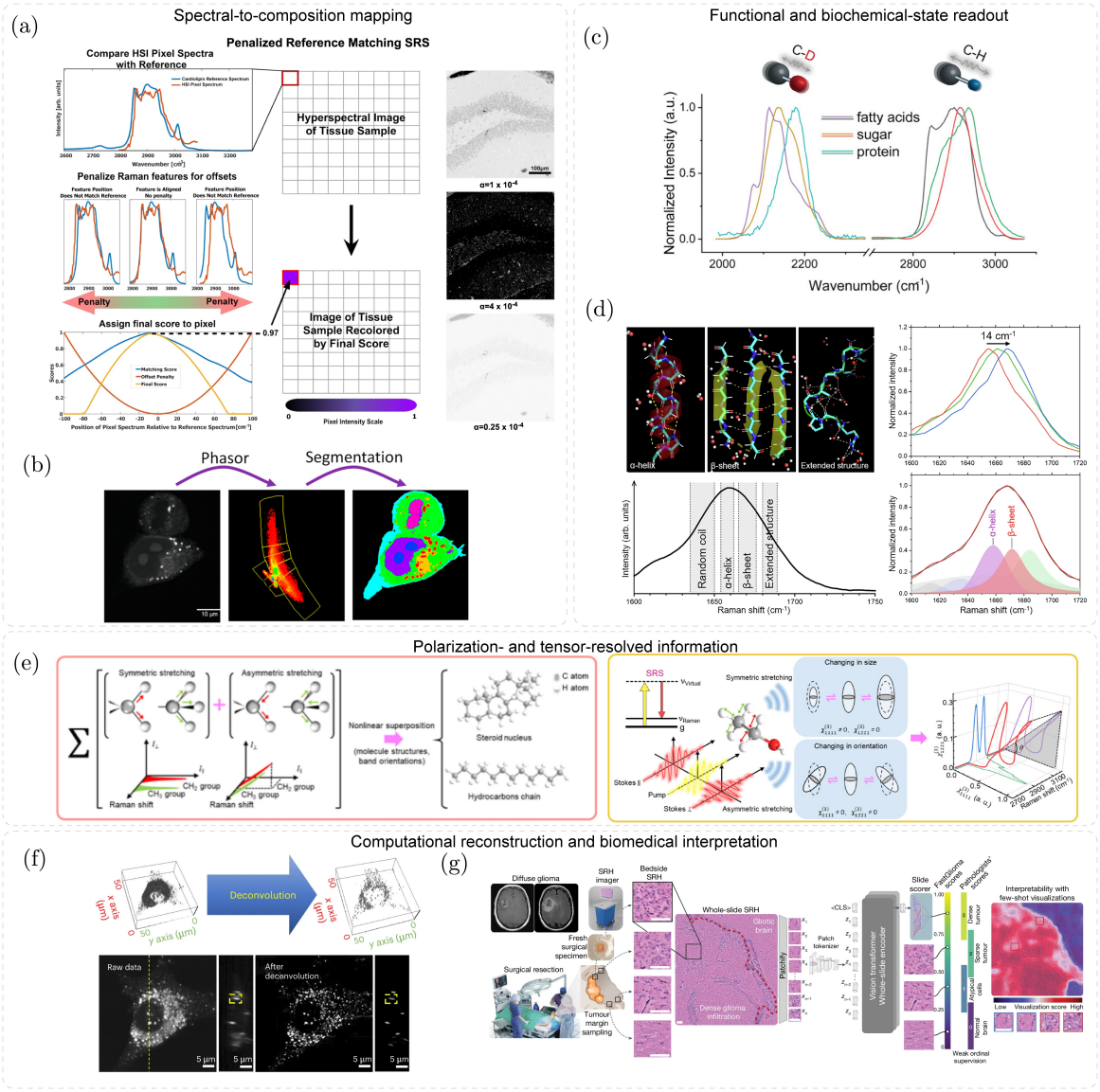

Fig. 5. Representative information-enhancement strategies organized by the type of information extracted from SRS measurements. (a) and (b) Spectral to composition mapping through PRM-SRS and spectral phasor analysis. Reproduced with permission from Refs. 136 and 160, respectively. (c) and (d) Functional and biochemical-state readout through isotope-traced metabolism and protein secondary-structure mapping. Reproduced with permission from Refs. 145 and 146, respectively. (e) Polarization- and tensor-resolved SRS reveals molecular orientational information. Adapted with permission from Ref. 151. (f) and (g) Computational reconstruction and biomedical interpretation through A-PoD recovery of latent spatial information and FastGlioma analysis of fresh surgical specimens. Adapted with permission from Ref. 132 and reproduced with permission from Ref. 154.

of intensity images into interpretable multicomponent chemical maps, although their performance still depends on assumptions about component number, spectral independence, nonnegativity, linear mixing, and the quality of reference spectra.

Phasor analysis offers another useful framework for spectral interpretation and unmixing (Fig. 5 (b)).[137,160] By projecting each pixel spectrum into a low-dimensional phasor space, it allows spectral relationships, cellular heterogeneity, and mixed biochemical states to be visualized without extensive model fitting.[161] Spectral phasor analysis has been applied to label-free multi-wavelength SRS for cellular biochemical response analysis and has more recently been extended to the cell-silent Raman region for unmixing overlapping C–D, alkyne, and other bio-orthogonal vibrational signals.[138]

Machine-learning-based unmixing is emerging as a flexible extension of these methods.[162] Autoencoders, physics-constrained models, and neural-network-based spectral decomposition can learn nonlinear relationships between measured spectra and underlying molecular components, which may be useful for noisy or highly overlapping spectra.[139,163] However, such methods require careful validation because learned components may not always correspond to physically meaningful molecular species.

Overall, spectral unmixing and computational molecular mapping expand SRS from bond-selective contrast imaging to multicomponent molecular analysis. The key challenge is not simply to acquire more spectral channels, but to convert those channels into reliable and biologically interpretable molecular information. Future developments will likely combine high-quality hyperspectral acquisition, curated reference libraries, physics-informed constraints, phasor visualization, and machine learning to improve chemical specificity while preserving quantitative reliability.

6.2. *Functional and biochemical-state readout*

Functional and biochemical-state readout represents a further level of information enhancement in SRS microscopy. While spectral unmixing separates molecular components, state-resolved SRS reports how those molecules are organized, metabolized, transported, or structurally transformed. This distinction is important because many biological processes are not defined only by molecular abundance. Lipid unsaturation, protein secondary structure, metabolic turnover, drug uptake, isotope incorporation, and water utilization all reflect biochemical states that cannot be fully captured by single-band intensity imaging.

Lipid imaging is a representative example of state-resolved SRS. Beyond mapping total lipid abundance through CH_2 stretching signals, hyperspectral and multiband SRS can distinguish saturated and unsaturated lipid features, characterize lipid droplet composition, and quantify lipid remodeling in cells and tissues. These readouts are valuable for studying fatty acid metabolism, membrane composition, lipid storage, steatosis, phospholipidosis, and disease-associated lipid dysregulation.[45,140,141,164–166] In this context, SRS transforms lipid contrast from a simple mass or density readout into a compositional and metabolic-state readout.

Isotope-assisted SRS further expands state-resolved imaging by reporting molecular turnover and metabolic activity. D2O-SRS detects newly synthesized biomolecules through deuterium incorporation into C–D bonds and has been used for *in situ* metabolic imaging in cells, tissues, and living animals.[142,143] Related isotope strategies include deuterated amino acid labeling for nascent protein synthesis and protein turnover, D2O metabolic incorporation for rapid single-bacterium antimicrobial susceptibility testing, and deuterated neurotransmitter imaging for tracking dopamine or GABA transport.[144,167] More recently, isotope-traced SRS has also been extended to plant biology, where D2O-SRS was used to monitor water metabolic flow in Arabidopsis, illustrating that isotope-assisted SRS can report biochemical dynamics across animals, microorganisms, neuronal systems, and plants (Fig. 5(c)).[145]

Bio-orthogonal Raman tags provide a complementary route to biochemical-state imaging. Alkyne-, nitrile-, and deuterium-labeled probes occupy the cell-silent Raman window and enable direct visualization of small molecules, metabolites, drugs, and biomolecular precursors with minimal endogenous background.[168,169] Alkyne-tag SRS has been used to track small biomolecules, drug distribution, and de novo synthesis of DNA, RNA, proteins, phospholipids, and triglycerides in living systems.[7,170,171] When combined with hyperspectral or multichannel SRS, these probes allow drug uptake, organelle targeting, pharmacodynamics, and metabolic remodeling to be monitored with chemical specificity.[172,173]

A particularly important recent advance is the use of hyperspectral SRS to image protein secondary structure in situ (Fig. 5(d)).[146] Conventional SRS protein imaging often relies on CH_3 or amide-band intensity as a proxy for protein abundance. By analyzing the amide I region, hyperspectral SRS can quantitatively map α-helix, β-sheet, turn, and disordered structures in protein condensates, enabling direct visualization of structural changes during phase separation and aggregation. This shifts SRS from protein-content imaging toward protein-structure and conformational-state imaging.

Overall, functional and biochemical-state readout broadens SRS from molecular composition mapping to functional molecular imaging. Lipid unsaturation, isotope incorporation, water metabolism, drug uptake, neurotransmitter transport, and protein secondary structure show that SRS can report not only where molecules are located, but also what biochemical state they occupy. The main challenges are spectral overlap, quantitative calibration, label or isotope perturbation, and biological validation of Raman-derived state markers.

6.3. *Polarization-, orientation-, and tensor-resolved information*

Polarization-, orientation-, and tensor-resolved SRS introduces an additional physical dimension into vibrational imaging. Conventional SRS usually records scalar intensity at selected Raman shifts, which mainly reflects the abundance of specific vibrational bonds. However, Raman scattering is governed by the molecular Raman tensor, and its polarization dependence contains information about molecular symmetry, orientation, anisotropy, and supramolecular organization. By controlling the polarization states of the pump and Stokes beams and analyzing polarization-dependent SRS signals, SRS can report not only molecular composition, but also molecular arrangement.

Early polarization-resolved SRS established the basic principle that Raman depolarization ratios can be obtained from SRS intensity ratios measured under different polarization configurations.[147] This provided a foundation for transferring polarization Raman concepts into high-speed nonlinear Raman microscopy. Later polarization-resolved and dual-polarization hyperspectral SRS methods extended this idea to imaging, allowing chemical composition and polarization-dependent structural information to be measured together.[174] Applications such as label-free tooth imaging demonstrated that polarization-sensitive SRS can reveal biomolecular composition as well as organization or orientation in structured biological materials.[148,149]

Orientation-sensitive SRS is especially valuable for anisotropic biological and pharmaceutical systems. In ordered samples such as membranes, lipid assemblies, myelin, collagen-rich tissues, crystals, and drug–membrane complexes, the SRS signal depends on the angle between excitation polarization and the dominant vibrational bond orientation. A representative example is polarization-sensitive SRS imaging of amphotericin B in Candida membranes. By probing the fingerprint C=C stretching vibration, this method visualized amphotericin B, ergosterol, and lipids in single fungal cells and resolved drug orientation in the membrane environment.[150] This illustrates how polarization contrast can reveal molecular organization and drug–membrane interactions that are difficult to obtain from intensity-only SRS images.

Recent tensor-resolved SRS further pushes polarization imaging beyond simple parallel/perpendicular intensity comparison. Quadrature phase-shifted polarization SRS enables rapid detection of polarized and depolarized Raman tensor components and has been used for high-specificity spatiotemporal cholesterol imaging (Fig. 5(e)).[151] This is important because chemically similar molecules may have overlapping Raman frequencies but distinct polarization or tensor responses. Tensor-resolved SRS therefore enhances molecular specificity by adding structural selection rules to spectral contrast.

Overall, polarization- and tensor-resolved SRS transforms vibrational imaging from scalar chemical mapping into multidimensional structural imaging. It complements spectral unmixing and biochemical-state readout by adding sensitivity to molecular orientation, symmetry, anisotropy, and packing order. Remaining challenges include polarization distortion from high-NA objectives, birefringence and scattering in biological samples, calibration of the focal polarization state, separation of concentration and orientation effects, and the need for fast polarization modulation compatible with live-cell imaging.[175] Future developments will likely combine rapid polarization encoding, hyperspectral acquisition, Raman tensor modeling, and computational reconstruction to map molecular organization in complex biological systems.

6.4. *Computational reconstruction, virtual staining, and decision-level biomedical interpretation*

Computational methods provide a higher-level route for information enhancement by transforming acquired SRS data into spatially refined, pathologist-readable, or machine-interpretable outputs

that are not directly available from the raw intensity images. This subsection covers three related but distinct levels of computational information extraction: model-based reconstruction of latent spatial features, virtual staining that translates molecular contrast into familiar histological representations, and AI-assisted interpretation that derives phenotypic, molecular, or diagnostic information. Although these approaches differ in their computational mechanisms and output types, they share the goal of converting measured vibrational data into richer and more accessible biomedical information.

Computational reconstruction can first enhance the spatial information recoverable from conventionally acquired SRS images. A representative example is Adam optimization-based pointillism deconvolution (A-PoD), which models a diffraction-limited SRS image as the convolution of a point-spread function with a distribution of virtual point sources and iteratively optimizes their positions. This post-acquisition reconstruction recovers super-resolved spatial information for nanoscale analysis of biomolecular distributions and subcellular metabolic activity (Fig. 5(f)).[132] Although its performance outcome is improved spatial resolution, A-PoD does not reshape the excitation field or modify the physical image-formation process during acquisition. It is therefore included here as computational recovery of latent spatial information, while its relationship to super-resolution SRS is also noted in Sec. 5.2.

SRH provides a key route for converting SRS molecular contrast into clinically interpretable histological information. By combining lipid- and protein-associated SRS signals, SRH can generate H&E-like virtual histology images from fresh, unprocessed surgical specimens without conventional fixation, sectioning, or staining.[100] This virtual-staining strategy bridges label-free vibrational microscopy with routine pathological interpretation by presenting SRS contrast in a familiar histological language. Deep-learning-based methods further improve this translation: single-shot femtosecond SRS histology enables rapid biopsy assessment, while stimulated Raman virtual FFPE staining uses a semi-supervised CycleGAN framework to transform fresh-tissue SRS images into FFPE-like histology appearances from unpaired training data.[98,155] Together, these approaches enhance the clinical compatibility of SRS by mapping label-free chemical information onto established pathological staining styles while preserving rapid and nondestructive tissue assessment. Similar virtual-staining strategies have also been explored in other label-free microscopy modalities.[176,177]

AI-assisted computational pathology goes beyond virtual staining by directly extracting diagnostic and molecular information from SRH images. Near-real-time AI-SRH combines SRH with deep neural networks for intraoperative brain tumor diagnosis, while DeepGlioma and FastGlioma extend this concept toward rapid molecular classification and glioma infiltration detection (Fig. 5(g)).[94,153,154,178] The development of large datasets such as OpenSRH further supports benchmarking, model training, and broader deployment of SRH-based computational pathology.[152] Beyond brain tumors, related AI-SRS/SRH workflows have also been explored for prostate, breast, lung, and cytology-related applications, suggesting that computational SRS pathology may expand across multiple disease contexts.[179–185]

Overall, computational reconstruction, virtual staining, and AI-assisted interpretation extend SRS information across spatial, representational, phenotypic, and decision-making levels. Model-based reconstruction recovers latent image features, virtual staining translates molecular contrast into familiar histological representations, and AI-assisted analysis derives clinically or biologically relevant outputs.[186,187] Key challenges include reconstruction fidelity, training-data quality, domain shift across instruments and institutions, neural-network interpretability, preservation of quantitative chemical meaning, regulatory validation, and prospective clinical testing.[188] Future SRS computational pathology will likely combine chemically grounded image formation, robust virtual staining, large-scale annotated datasets, foundation models, and human-in-the-loop validation.

7. Challenges and Future Perspectives

The recent development of SRS microscopy shows that enhancement is no longer a single-parameter problem. Improving sensitivity, speed, depth, resolution, molecular specificity, and interpretability often requires coordinated advances in laser engineering, optical design, detection, sample preparation, chemical labeling, and computation. The four enhancement routes discussed in this review —

signal enhancement, acquisition enhancement, light-field enhancement, and information enhancement — should therefore be viewed not as isolated categories, but as interconnected strategies for increasing the amount of reliable molecular information that SRS microscopy can deliver.

A first challenge is the balance between sensitivity and sample perturbation. Higher laser power, longer dwell time, resonance enhancement, plasmonic enhancement, or stronger nonlinear excitation can improve weak SRS signals, but may also introduce photodamage, heating, or biological perturbation. Future signal-enhanced SRS should therefore combine low-noise sources, optimized modulation, balanced detection, computational denoising, and careful phototoxicity evaluation, especially for live-cell, organoid, and *in vivo* studies.[189–191]

A second challenge is the trade-off between speed and spectral bandwidth. Single-frequency SRS enables fast imaging of predefined contrasts, whereas hyperspectral and broadband SRS provide richer molecular information at the cost of longer acquisition, more complex encoding, and heavier data processing. Future acquisition-enhanced SRS should move toward task-adaptive sampling: sparse spectral selection, rapid wavelength tuning, time encoding, multiplex modulation, and reconstruction algorithms should be designed around the biological question rather than the goal of collecting the largest possible dataset.[192]

Deep-tissue and volumetric SRS imaging face coupled challenges in scattering, aberration, photodose, and quantitative accuracy. Bessel beams, tomography, phase-controlled focusing, adaptive optics, epi-detection, and tissue clearing have improved access to thick specimens, but none of them removes the need for calibration. Future deep SRS systems should report imaging depth, resolution, signal-to-noise ratio, and reconstruction uncertainty in a more standardized way, so that depth enhancement can be evaluated quantitatively rather than visually.

As SRS readouts become increasingly multidimensional, standardization and interpretability become essential. Hyperspectral, isotope-assisted, polarization-resolved, tensor-resolved, and AI-processed SRS data can reveal rich molecular information, but they also increase the risk of ambiguous or model-dependent interpretation. Future information-enhanced SRS will require curated reference spectra, standardized preprocessing, uncertainty estimation, open datasets, and interpretable algorithms that preserve the connection between Raman signal, molecular origin, and biological conclusion.[193–195]

Another major challenge is system complexity and translational usability. Many enhanced SRS methods rely on sophisticated lasers, precise synchronization, specialized modulation, adaptive optics, custom probes, or advanced reconstruction pipelines. These methods are powerful, but their broader impact will depend on whether they can be made stable, compact, automated, and reproducible. Future platforms should prioritize robust laser sources, simplified alignment, integrated calibration, user-friendly software, and compatibility with realistic biological and clinical workflows.

Overall, the future of SRS microscopy will depend on how well these trade-offs are balanced. The most impactful systems may not be those that maximize a single metric, but those that deliver reliable molecular information under practical constraints. By integrating signal, acquisition, light-field, and information enhancement, SRS microscopy can continue to evolve from a powerful vibrational imaging technique into a robust, quantitative, and interpretable molecular imaging platform for biology, pathology, and precision medicine.

Acknowledgments

We acknowledge financial support from the National Key R&D Program of China (2021YFF0502900); National Natural Science Foundation of China (62425501); Municipal Natural Science Foundation of Shanghai (23dz2260100); Medical Engineering Fund of Fudan University (yg2025-general-16); and Shanghai Key Laboratory of Female Reproductive Endocrine Related Diseases.

Yingjie He and Qingjun Meng contributed equally to this work.

Conflicts of Interest

The authors declare that there are no conflicts of interest relevant to this paper.

Supplementary Materials

The Supplemental Materials are available at: https://www.worldscientific.com/doi/suppl/10.1142/S1793545826300181

ORCID

Yingjie He https://orcid.org/0009-0009-3328-8446
Qingjun Meng https://orcid.org/0009-0007-6714-0672
Minbiao Ji https://orcid.org/0000-0002-9066-4008

References

1. C. W. Freudiger *et al.*, "Label-free biomedical imaging with high sensitivity by stimulated Raman scattering microscopy," *Science* **322**(5909), 1857–1861 (2008).
2. R. Ranjan, L. Sirleto, "Stimulated Raman scattering microscopy: A review," *Photonics* **11**, 489 (2024).
3. B. G. Saar *et al.*, "Video-rate molecular imaging *in vivo* with stimulated Raman scattering," *Science* **330**(6009), 1368–1370 (2010).
4. D. Fu *et al.*, "Quantitative chemical imaging with multiplex stimulated Raman scattering microscopy," *J. Am. Chem. Soc.* **134**(8), 3623–3626 (2012).
5. W. Min, J.-X. Cheng, Y. Ozeki, "Theory, innovations and applications of stimulated Raman scattering microscopy," *Nat. Photonics* **19**(8), 803–816 (2025).
6. L. Shi *et al.*, "Optical imaging of metabolic dynamics in animals," *Nat. Commun.* **9**(1), 2995 (2018).
7. L. Wei *et al.*, "Live-cell imaging of alkyne-tagged small biomolecules by stimulated Raman scattering," *Nat. Methods* **11**(4), 410–412 (2014).
8. M. Ji *et al.*, "Rapid, label-free detection of brain tumors with stimulated Raman scattering microscopy," *Sci. Transl. Med.* **5**(201), 201ra119–201ra119 (2013).
9. M. Ji *et al.*, "Detection of human brain tumor infiltration with quantitative stimulated Raman scattering microscopy," *Sci. Transl. Med.* **7**(309), 309ra163–309ra163 (2015).
10. W. Zhao *et al.*, "Dynamic tracking of lipid metabolism in live tumor spheroids by bioorthogonal stimulated Raman scattering microscopy," *J. Innov. Opt. Health Sci.* **19**, 2650003 (2026).
11. X. Audier *et al.*, "Noise in stimulated Raman scattering measurement: From basics to practice," *APL Photonics* **5**(1), 011101 (2020).
12. Y. Ozeki *et al.*, "Analysis and experimental assessment of the sensitivity of stimulated Raman scattering microscopy," *Opt. Express* **17**(5), 3651–3658 (2009).
13. L. Genchi, S. P. Laptenok, C. Liberale, "Background signals in stimulated Raman scattering microscopy and current solutions to avoid them," *Adv. Phys. X* **8**(1), 2176258 (2023).
14. D. Fu *et al.*, "Hyperspectral imaging with stimulated Raman scattering by chirped femtosecond lasers," *J. Phys. Chem. B* **117**(16), 4634–4640 (2013).
15. C. W. Freudiger *et al.*, "Stimulated Raman scattering microscopy with a robust fibre laser source," *Nat. Photonics* **8**(2), 153–159 (2014).
16. S. Karpf *et al.*, "A time-encoded technique for fibre-based hyperspectral broadband stimulated Raman microscopy," *Nat. Commun.* **6**(1), 6784 (2015).
17. A. H. Hill, B. Manifold, D. Fu, "Tissue imaging depth limit of stimulated Raman scattering microscopy," *Biomed. Opt. Express* **11**(2), 762–774 (2020).
18. W. J. Tipping, K. Faulds, D. Graham, "Advances in super-resolution stimulated Raman scattering microscopy," *Chem. Biomed. Imaging* **2**(11), 733–743 (2024).
19. D. Zhang *et al.*, "Quantitative vibrational imaging by hyperspectral stimulated Raman scattering microscopy and multivariate curve resolution analysis," *Anal. Chem.* **85**(1), 98–106 (2013).
20. J. Duboisset *et al.*, "Molecular orientational order probed by coherent anti-Stokes Raman scattering (CARS) and stimulated Raman scattering (SRS) microscopy: A spectral comparative study," *J. Phys. Chem. B* **119**, 3242–3249 (2015).
21. Y. Yu *et al.*, "AI-assisted coherent Raman scattering microscopy for clinical translation," *Chem. Biomed. Imaging* **4**(6), 970 (2026).
22. L. Wei *et al.*, "Super-multiplex vibrational imaging," *Nature* **544**(7651), 465–470 (2017).
23. P. Berto, E. R. Andresen, H. Rigneault, "Background-free stimulated Raman spectroscopy and microscopy," *Phys. Rev. Lett.* **112**(5), 053905 (2014).
24. B. Manifold *et al.*, "Denoising of stimulated Raman scattering microscopy images via deep learning," *Biomed. Opt. Express* **10**(8), 3860–3874 (2019).
25. F.-K. Lu *et al.*, "Multicolor stimulated Raman scattering microscopy," *Mol. Phys.* **110**(15–16), 1927–1932 (2012).

26. H. Lin *et al.*, "Spectroscopic stimulated Raman scattering imaging of highly dynamic specimens through matrix completion," *Light Sci. Appl.* **7**(5), 17179–17179 (2018).
27. X. Chen *et al.*, "Volumetric chemical imaging by stimulated Raman projection microscopy and tomography," *Nat. Commun.* **8**(1), 15117 (2017).
28. J. Ao *et al.*, "Photoswitchable vibrational nanoscopy with sub-100-nm optical resolution," *Adv. Photonics* **5**(6), 066001 (2023).
29. M. K. Krishnan Nambudiri *et al.*, "Artificial intelligence-assisted stimulated Raman histology: New frontiers in vibrational tissue imaging," *Cancers (Basel)* **16**(23), 3917 (2024).
30. C. Zhang, D. Zhang, J.-X. Cheng, "Coherent Raman scattering microscopy in biology and medicine," *Annu. Rev. Biomed. Eng.* **17**(1), 415–445 (2015).
31. D. Zhang, M. N. Slipchenko, J.-X. Cheng, "Highly sensitive vibrational imaging by femtosecond pulse stimulated Raman loss," *J. Phys. Chem. Lett.* **2**(11), 1248–1253 (2011).
32. P. Nandakumar, A. Kovalev, A. Volkmer, "Vibrational imaging based on stimulated Raman scattering microscopy," *New J. Phys.* **11**(3), 033026 (2009).
33. J.-X. Cheng, X. S. Xie, "Vibrational spectroscopic imaging of living systems: An emerging platform for biology and medicine," *Science* **350**(6264), aaa8870 (2015).
34. L. Wei *et al.*, "Live-cell bioorthogonal chemical imaging: Stimulated Raman scattering microscopy of vibrational probes," *Acc. Chem. Res.* **49**(8), 1494–1502 (2016).
35. Z. Chen *et al.*, "Multicolor live-cell chemical imaging by isotopically edited alkyne vibrational palette," *J. Am. Chem. Soc.* **136**(22), 8027–8033 (2014).
36. L. Zhang *et al.*, "Spectral tracing of deuterium for imaging glucose metabolism," *Nat. Biomed. Eng.* **3**(5), 402–413 (2019).
37. Y. R. Shen, N. Bloembergen, "Theory of stimulated Brillouin and Raman scattering," *Phys. Rev.* **137**(6A), A1787–A1805 (1965).
38. Y.-R. Shen, *The Principles of Nonlinear Optics* (Wiley-Interscience, New York, 1984).
39. R. C. Prince, R. R. Frontiera, E. O. Potma, "Stimulated Raman scattering: From bulk to nano," *Chem. Rev.* **117**(7), 5070–5094 (2017).
40. W. M. Tolles *et al.*, "A review of the theory and application of coherent anti-Stokes Raman spectroscopy (CARS)," *Appl. Spectrosc.* **31**(4), 253–271 (1977).
41. C. L. Evans, E. O. Potma, X. S. Xie, "Coherent anti-Stokes Raman scattering spectral interferometry: Determination of the real and imaginary components of nonlinear susceptibility $\chi(3)$ for vibrational microscopy," *Opt. Lett.* **29** (24), 2923–2925 (2004).
42. S. Li *et al.*, "Coherent anti-Stokes Raman scattering microscopy and its applications," *Front. Phys.* **8**, 598420 (2020).
43. C. H. Camp, Y. J. Lee, M. T. Cicerone, "Quantitative, comparable coherent anti-Stokes Raman scattering (CARS) spectroscopy: Correcting errors in phase retrieval," *J. Raman Spectrosc.* **47**, 408–415 (2016).
44. S. Oh *et al.*, "Protein and lipid mass concentration measurement in tissues by stimulated Raman scattering microscopy," *Proc. Natl. Acad. Sci. USA* **119**(17), e2117938119 (2022).
45. D. Fu *et al.*, "*In vivo* metabolic fingerprinting of neutral lipids with hyperspectral stimulated Raman scattering microscopy," *J. Am. Chem. Soc.* **136**(24), 8820–8828 (2014).
46. B. G. Saar *et al.*, "Imaging drug delivery to skin with stimulated Raman scattering microscopy," *Mol. Pharm.* **8**(3), 969–975 (2011).
47. P. Wang *et al.*, "Mechanisms of epi-detected stimulated Raman scattering microscopy," *IEEE J. Sel. Top. Quantum Electron.* **18**(1), 384–388 (2012).
48. Y. Li *et al.*, "Review on multimodal nonlinear optical microscopy imaging technology," *Acta Opt. Sin.* **44**(4), 0400002 (2024).
49. Y. Ozeki *et al.*, "High-speed molecular spectral imaging of tissue with stimulated Raman scattering," *Nat. Photonics* **6**(12), 845–851 (2012).
50. C.-S. Liao *et al.*, "Stimulated Raman spectroscopic imaging by microsecond delay-line tuning," *Optica* **3**(12), 1377–1380 (2016).
51. T. Hellerer, A. M. Enejder, A. Zumbusch, "Spectral focusing: High spectral resolution spectroscopy with broad-bandwidth laser pulses," *Appl. Phys. Lett.* **85**(1), 25–27 (2004).
52. A. De la Cadena *et al.*, "Broadband stimulated Raman imaging based on multi-channel lock-in detection for spectral histopathology," *APL Photonics* **7**(7), 076104 (2022).
53. L. Kong *et al.*, "Multicolor stimulated Raman scattering microscopy with a rapidly tunable optical parametric oscillator," *Opt. Lett.* **38**(2), 145–147 (2013).
54. H. Ni *et al.*, "Multiwindow SRS imaging using a rapid widely tunable fiber laser," *Anal. Chem.* **93**(47), 15703–15711 (2021).
55. K. Nose *et al.*, "Sensitivity enhancement of fiber-laser-based stimulated Raman scattering microscopy by collinear balanced detection technique," *Opt. Express* **20**(13), 13958–13965 (2012).

56. F. Crisafi *et al.*, "In-line balanced detection stimulated Raman scattering microscopy," *Sci. Rep.* **7**(1), 10745 (2017).
57. D. X. Lioe *et al.*, "A stimulated Raman scattering CMOS pixel using a high-speed charge modulator and lock-in amplifier," *Sensors* **16**(4), 532 (2016).
58. C. S. Liao *et al.*, "Denoising stimulated Raman spectroscopic images by total variation minimization," *J. Phys. Chem. C Nanomater. Interfaces* **119**(33), 19397–19403 (2015).
59. P. Abdolghader *et al.*, "Unsupervised hyperspectral stimulated Raman microscopy image enhancement: Denoising and segmentation via one-shot deep learning," *Opt. Express* **29**(21), 34205–34219 (2021).
60. G. Ding *et al.*, "Self-supervised elimination of non-independent noise in hyperspectral imaging," *Newton* **1**(6), 100195 (2025).
61. L. Wei, W. Min, "Electronic preresonance stimulated Raman scattering microscopy," *J. Phys. Chem. Lett.* **9**(15), 4294–4301 (2018).
62. Y. Bi *et al.*, "Near-resonance enhanced label-free stimulated Raman scattering microscopy with spatial resolution near 130 nm," *Light Sci. Appl.* **7**(1), 81 (2018).
63. H. Lin *et al.*, "Label-free nanoscopy of cell metabolism by ultrasensitive reweighted visible stimulated Raman scattering," *Nat. Methods* **22**(5), 1040–1050 (2025).
64. A. Colazo *et al.*, "Visible enhanced stimulated Raman scattering microscopy via frequency-doubling of picosecond pulses," *Biomed. Opt. Express* **16**(6), 2430–2439 (2025).
65. J. Du *et al.*, "Computational design of molecular probes for electronic preresonance Raman scattering microscopy," *J. Phys. Chem. B* **127**(22), 4979–4988 (2023).
66. C. Zong *et al.*, "Plasmon-enhanced stimulated Raman scattering microscopy with single-molecule detection sensitivity," *Nat. Commun.* **10**(1), 5318 (2019).
67. C. Zong, J.-X. Cheng, "Origin of dispersive line shapes in plasmon-enhanced stimulated Raman scattering microscopy," *Nanophotonics* **10**(1), 617–625 (2020).
68. Y. Zhu *et al.*, "Stimulated Raman photothermal microscopy toward ultrasensitive chemical imaging," *Sci. Adv.* **9**(43), eadi2181 (2023).
69. Y. Zhu *et al.*, "Stimulated Raman photothermal microscopy: Theory and implementation," *Adv. Opt. Photon.* **18**(2), 369–420 (2026).
70. X. Ge *et al.*, "Fiber laser based stimulated Raman photothermal microscopy towards a high-performance and user-friendly chemical imaging platform," *PhotoniX* **6**(1), 35 (2025).
71. C. A. Casacio *et al.*, "Quantum-enhanced nonlinear microscopy," *Nature* **594**(7862), 201–206 (2021).
72. Z. Xu *et al.*, "Quantum-enhanced stimulated Raman scattering microscopy in a high-power regime," *Opt. Lett.* **47**(22), 5829–5832 (2022).
73. A. Terrasson *et al.*, "Fast biological imaging with quantum-enhanced Raman microscopy," *Opt. Express* **32**(21), 36193–36206 (2024).
74. J. Wu *et al.*, "Cavity-enhanced stimulated Raman scattering from short GaP nanowires," *Nano Lett.* **9**(9), 3252–3257 (2009).
75. J. F. McMillan *et al.*, "Enhanced stimulated Raman scattering in slow-light photonic crystal waveguides," *2006 Conf. Lasers and Electro-Optics and 2006 Quantum Electronics and Laser Science Conf.*, pp. 1–2 (IEEE, 2006).
76. Y. Ozeki *et al.*, "Stimulated Raman scattering microscope with shot noise limited sensitivity using subharmonically synchronized laser pulses," *Opt. Express* **18**(13), 13708–13719 (2010).
77. K. Mars *et al.*, "Label-free biomedical imaging using high-speed lock-in pixel sensor for stimulated Raman scattering," *Sensors* **17**(11), 2581 (2017).
78. Y. Choi *et al.*, "Shot-noise-limited two-color stimulated Raman scattering microscopy with a balanced detection scheme," *J. Phys. Chem. B* **124**(13), 2591–2599 (2020).
79. C. Riek *et al.*, "Stimulated Raman scattering microscopy by Nyquist modulation of a two-branch ultrafast fiber source," *Opt. Lett.* **41**(16), 3731–3734 (2016).
80. C. W. Freudiger *et al.*, "Highly specific label-free molecular imaging with spectrally tailored excitation-stimulated Raman scattering (STE-SRS) microscopy," *Nat. Photonics* **5**(2), 103–109 (2011).
81. A. H. Hill *et al.*, "Frequency modulation stimulated Raman scattering microscopy through polarization encoding," *J. Phys. Chem. B* **123**(40), 8397–8404 (2019).
82. L. Genchi *et al.*, "Broadband background-free stimulated Raman scattering microspectroscopy with a novel frequency modulation scheme," *APL Photonics* **9**(12), 126112 (2024).
83. H. Xie *et al.*, "Deep learning-assisted reconstruction of Raman speckle images transmitted through biological tissues," *J. Innov. Opt. Health Sci.* **19**, 2640008 (2026).
84. Y. Xu *et al.*, "A self-supervised learning-based method for simultaneous motion artifacts removal and denoising of OCTA images," *J. Innov. Opt. Health Sci.* **19**, 2540006 (2026).
85. F. Hu *et al.*, "Supermultiplexed optical imaging and barcoding with engineered polyynes," *Nat. Methods* **15**(3), 194–200 (2018).

86. N. Qian, W. Min, "Super-multiplexed vibrational probes: Being colorful makes a difference," *Curr. Opin. Chem. Biol.* **67**, 102115 (2022).
87. L. Shi *et al.*, "Electronic resonant stimulated Raman scattering micro-spectroscopy," *J. Phys. Chem. B* **122**(39), 9218–9224 (2018).
88. S. Oh *et al.*, "Fluorescence-free single-molecule microscopy via electronic resonance stimulated Raman scattering," *Nat. Commun.* **17**, 2720 (2026).
89. C. Zong *et al.*, "Plasmon-enhanced coherent anti-Stokes Raman scattering vs plasmon-enhanced stimulated Raman scattering: Comparison of line shape and enhancement factor," *J. Chem. Phys.* **154**(3), 034201 (2021).
90. S. Adhikari *et al.*, "Photothermal microscopy: Imaging the optical absorption of single nanoparticles and single molecules," *ACS Nano* **14**(12), 16414–16445 (2020).
91. Y. Michael *et al.*, "Squeezing-enhanced Raman spectroscopy," *npj Quantum Inf.* **5**(1), 81 (2019).
92. R. B. de Andrade *et al.*, "Quantum-enhanced continuous-wave stimulated Raman scattering spectroscopy," *Optica* **7**(5), 470–475 (2020).
93. D. Agarwal *et al.*, "Nanocavity-enhanced giant stimulated Raman scattering in Si nanowires in the visible light region," *Nano Lett.* **19**(2), 1204–1209 (2019).
94. T. C. Hollon *et al.*, "Near real-time intraoperative brain tumor diagnosis using stimulated Raman histology and deep neural networks," *Nat. Med.* **26**(1), 52–58 (2020).
95. A. De la Cadena *et al.*, "Multiplex chemical imaging based on broadband stimulated Raman scattering microscopy," *J. Vis. Exp.* **185**, 1–25 (2022).
96. R. He *et al.*, "Stimulated Raman scattering microscopy and spectroscopy with a rapid scanning optical delay line," *Opt. Lett.* **42**(4), 659–662 (2017).
97. K. Bae, W. Zheng, Z. Huang, "Spatial light-modulated stimulated Raman scattering (SLM-SRS) microscopy for rapid multiplexed vibrational imaging," *Theranostics* **10**(1), 312–322 (2020).
98. Z. Liu *et al.*, "Instant diagnosis of gastroscopic biopsy via deep-learned single-shot femtosecond stimulated Raman histology," *Nat. Commun.* **13**(1), 4050 (2022).
99. T. Würthwein *et al.*, "Multi-color stimulated Raman scattering with a frame-to-frame wavelength-tunable fiber-based light source," *Biomed. Opt. Express* **12**(10), 6228–6236 (2021).
100. D. A. Orringer *et al.*, "Rapid intraoperative histology of unprocessed surgical specimens via fibre-laser-based stimulated Raman scattering microscopy," *Nat. Biomed. Eng.* **1**(2), 0027 (2017).
101. C. Kong *et al.*, "High-contrast, fast chemical imaging by coherent Raman scattering using a self-synchronized two-colour fibre laser," *Light Sci. Appl.* **9**(1), 25 (2020).
102. S. Heuke *et al.*, "Simultaneous dual-channel stimulated Raman scattering microscopy demultiplexed at distinct modulation frequencies," *Opt. Lett.* **43**(15), 3582–3585 (2018).
103. B. Zhang *et al.*, "Rapid, large-scale stimulated Raman histology with strip mosaicing and dual-phase detection," *Biomed. Opt. Express* **9**(6), 2604–2613 (2018).
104. R. He *et al.*, "Dual-phase stimulated Raman scattering microscopy for real-time two-color imaging," *Optica* **4**(1), 44–47 (2016).
105. B. Shen *et al.*, "Simultaneous dual-Raman-shift scanning-free stimulated Raman scattering microscopy for label-free biomolecular imaging," *Nat. Commun.* **17**, 6607 (2026).
106. M. S. Alshaykh *et al.*, "High-speed stimulated hyperspectral Raman imaging using rapid acousto-optic delay lines," *Opt. Lett.* **42**(8), 1548–1551 (2017).
107. H. Lin *et al.*, "Microsecond fingerprint stimulated Raman spectroscopic imaging by ultrafast tuning and spatial-spectral learning," *Nat. Commun.* **12**(1), 3052 (2021).
108. J. Réhault *et al.*, "Broadband stimulated Raman scattering with Fourier-transform detection," *Opt. Express* **23**(19), 25235–25246 (2015).
109. F. X. Xu, E. G. Rathbone, D. Fu, "Simultaneous dual-band hyperspectral stimulated Raman scattering microscopy with femtosecond optical parametric oscillators," *J. Phys. Chem. B* **127**(10), 2187–2197 (2023).
110. I. J. Pence *et al.*, "Multi-window sparse spectral sampling stimulated Raman scattering microscopy," *Biomed. Opt. Express* **12**(10), 6095–6114 (2021).
111. W. Liang *et al.*, "Deep learning-driven computational imaging for light field microscopy," *J. Innov. Opt. Health Sci.* **19**, 2630008 (2026).
112. X. Chen *et al.*, "Accelerated stimulated Raman projection tomography by sparse reconstruction from sparse-view data," *IEEE Trans. Biomed. Eng.* **67**(5), 1293–1302 (2019).
113. P. Lin *et al.*, "Tilt-angle stimulated Raman projection tomography," *Opt. Express* **30**(20), 37112–37123 (2022).
114. W. Wang, Z. Huang, "Stimulated Raman scattering tomography for rapid three-dimensional chemical imaging of cells and tissue," *Adv. Photonics* **6**(2), 026001–026001 (2024).
115. S. Lin, L. Gong, Z. Huang, "Time-of-flight resolved stimulated Raman scattering microscopy using counter-propagating ultraslow Bessel light bullets generation," *Light Sci. Appl.* **13**(1), 148 (2024).

116. L. Gong *et al.*, "Saturated stimulated-Raman-scattering microscopy for far-field superresolution vibrational imaging," *Phys. Rev. Appl.* **11**(3), 034041 (2019).
117. X. Lv *et al.*, "Super-resolution stimulated Raman scattering microscopy with the phase-shifted spatial frequency modulation," *Opt. Lett.* **47**(17), 4552–4555 (2022).
118. J. Shou *et al.*, "Super-resolution vibrational imaging based on photoswitchable Raman probe," *Sci. Adv.* **9**(24), eade9118 (2023).
119. J. I. Kim *et al.*, "4Pi stimulated Raman scattering for label-free super-resolution chemical imaging," *Sci. Adv.* **12**(1), eaec0523 (2026).
120. K. Bae *et al.*, "Epi-detected hyperspectral stimulated Raman scattering microscopy for label-free molecular subtyping of glioblastomas," *Anal. Chem.* **90**(17), 10249–10255 (2018).
121. W. Wang, Z. Huang, "Stimulated Raman scattering microscopy with phase-controlled light focusing and aberration correction for rapid and label-free, volumetric deep tissue imaging," *Opto-Electron. Adv.* **7**(9), 240064 (2024).
122. S. K. Luna *et al.*, "Adaptive optics stimulated Raman scattering microscopy for topical product pharmacokinetic imaging," *Biomed. Opt. Express* **17**(1), 125–144 (2025).
123. W. Wang, Z. Huang, "Polychromatic adaptive optics-assisted stimulated Raman scattering microscopy enables deep tissue chemical imaging," *Laser Photonics Rev.* **19**(24), e01022 (2025).
124. D. S. Richardson, J. W. Lichtman, "Clarifying tissue clearing," *Cell* **162**(2), 246–257 (2015).
125. M. Wei *et al.*, "Volumetric chemical imaging by clearing-enhanced stimulated Raman scattering microscopy," *Proc. Natl. Acad. Sci. USA* **116**(14), 6608–6617 (2019).
126. L. Shi *et al.*, "Highly-multiplexed volumetric mapping with Raman dye imaging and tissue clearing," *Nat. Biotechnol.* **40**(3), 364–373 (2022).
127. J. Li *et al.*, "Volumetric stimulated Raman scattering imaging of cleared tissues towards three-dimensional chemical histopathology," *Biomed. Opt. Express* **10**(8), 4329–4339 (2019).
128. L. Wang *et al.*, "Direct measurement and optimization of the polarization-dependent modulation depth in super-resolution structured illumination microscopy," *J. Innov. Opt. Health Sci.* **18**(04), 2550005 (2025).
129. P. Xu *et al.*, "Advances in fluorescent nanoprobes for live-cell super-resolution imaging," *J. Innov. Opt. Health Sci.* **18**(03), 2530001 (2025).
130. J. Ao *et al.*, "Switchable stimulated Raman scattering microscopy with photochromic vibrational probes," *Nat. Commun.* **12**(1), 3089 (2021).
131. Y. Yang, X. Bai, F. Hu, "Photoswitchable polyynes for multiplexed stimulated Raman scattering microscopy with reversible light control," *Nat. Commun.* **15**(1), 2578 (2024).
132. H. Jang *et al.*, "Super-resolution SRS microscopy with A-PoD," *Nat. Methods* **20**(3), 448–458 (2023).
133. L. Shi *et al.*, "Super-resolution vibrational imaging using expansion stimulated Raman scattering microscopy," *Adv. Sci.* **9**(20), 2200315 (2022).
134. R. Espinoza, B. Wong, D. Fu, "Real-time, two-color stimulated Raman scattering imaging of mouse brain for tissue diagnosis," *J. Vis. Exp.* **180**, e63484 (2022).
135. Y. Zhou, W. Lu, H. J. Lee, "Recent advances in nonlinear optical techniques for metastatic melanoma diagnosis and mechanistic studies," *J. Innov. Opt. Health Sci.* **19**, 2544002 (2025).
136. W. Zhang *et al.*, "Multi-molecular hyperspectral PRM-SRS microscopy," *Nat. Commun.* **15**(1), 1599 (2024).
137. W. J. Tipping *et al.*, "Stimulated Raman scattering microscopy with spectral phasor analysis: Applications in assessing drug-cell interactions," *Chem. Sci.* **13**(12), 3468–3476 (2022).
138. W. J. Tipping *et al.*, "Unmixing hyperspectral SRS images in the cell-silent region of the Raman spectrum using phasor analysis," *Chem. Biomed. Imaging* **3**(9), 630–635 (2025).
139. D. Georgiev *et al.*, "Hyperspectral unmixing for Raman spectroscopy via physics-constrained autoencoders," *Proc. Natl. Acad. Sci. USA* **121** (45), e2407439121 (2024).
140. A. Rensonnet *et al.*, "Spectral fingerprinting of cellular lipid droplets using stimulated Raman scattering microscopy and chemometric analysis," *Analyst* **149**(2), 553–562 (2024).
141. J. Li *et al.*, "Lipid desaturation is a metabolic marker and therapeutic target of ovarian cancer stem cells," *Cell Stem Cell* **20**(3), 303–314 (2017).
142. L. Wei *et al.*, "Vibrational imaging of newly synthesized proteins in live cells by stimulated Raman scattering microscopy," *Proc. Natl. Acad. Sci. USA* **110**(28), 11226–11231 (2013).
143. L. Wei *et al.*, "Imaging complex protein metabolism in live organisms by stimulated Raman scattering microscopy with isotope labeling," *ACS Chem. Biol.* **10**(3), 901–908 (2015).
144. M. Zhang *et al.*, "Rapid determination of antimicrobial susceptibility by stimulated Raman scattering imaging of D_2O metabolic incorporation in a single bacterium," *Adv. Sci.* **7**(19), 2001452 (2020).
145. S. Bi *et al.*, "Imaging metabolic flow of water in plants with isotope-traced stimulated Raman

scattering microscopy," *Adv. Sci.* **11**(42), 2407543 (2024).
146. R. Sun *et al.*, "*In situ* secondary structure imaging of protein phase separation and aggregation by hyperspectral stimulated Raman scattering microscopy," *Nat. Commun.* **16**(1), 8552 (2025).
147. F. Munhoz *et al.*, "Polarization resolved stimulated Raman scattering: Probing depolarization ratios of liquids," *J. Raman Spectrosc.* **43**(3), 419–424 (2012).
148. Z. Wang *et al.*, "Polarization-resolved hyperspectral stimulated Raman scattering microscopy for label-free biomolecular imaging of the tooth," *Appl. Phys. Lett.* **108**(3), 033701 (2016).
149. Z. Wang *et al.*, "Optical diagnosis and characterization of dental caries with polarization-resolved hyperspectral stimulated Raman scattering microscopy," *Biomed. Opt. Express* **7**(4), 1284–1293 (2016).
150. P.-T. Dong *et al.*, "Polarization-sensitive stimulated Raman scattering imaging resolves amphotericin B orientation in Candida membrane," *Sci. Adv.* **7**(2), eabd5230 (2021).
151. Y. Zhang *et al.*, "High-specificity spatiotemporal cholesterol detection by quadrature phase-shifted polarization stimulated Raman imaging," *Angew. Chem. Int. Ed.* **64**(32), e202505038 (2025).
152. C. Jiang *et al.*, "OpenSRH: Optimizing brain tumor surgery using intraoperative stimulated Raman histology," *Advances in Neural Information Processing Systems*, Vol. 35, pp. 28502–28516, Curran Associates (2022).
153. T. Hollon *et al.*, "Artificial-intelligence-based molecular classification of diffuse gliomas using rapid, label-free optical imaging," *Nat. Med.* **29**(4), 828–832 (2023).
154. A. Kondepudi *et al.*, "Foundation models for fast, label-free detection of glioma infiltration," *Nature* **637**(8045), 439–445 (2025).
155. Z. Liu *et al.*, "Virtual formalin-fixed and paraffin-embedded staining of fresh brain tissue via stimulated Raman CycleGAN model," *Sci. Adv.* **10**(13), eadn3426 (2024).
156. L. Zhang *et al.*, "Rapid histology of laryngeal squamous cell carcinoma with deep-learning based stimulated Raman scattering microscopy," *Theranostics* **9**(9), 2541 (2019).
157. F. Masia *et al.*, "Hyperspectral image analysis for CARS, SRS, and Raman data," *J. Raman Spectrosc.* **46**(8), 727–734 (2015).
158. I. Chitra Ragupathy, V. Schweikhard, A. Zumbusch, "Multivariate analysis of hyperspectral stimulated Raman scattering microscopy images," *J. Raman Spectrosc.* **52**(9), 1630–1642 (2021).
159. E. W. Hislop *et al.*, "Label-free imaging of lipid droplets in prostate cells using stimulated Raman scattering microscopy and multivariate analysis," *Anal. Chem.* **94**(25), 8899–8908 (2022).
160. D. Fu, X. S. Xie, "Reliable cell segmentation based on spectral phasor analysis of hyperspectral stimulated Raman scattering imaging data," *Anal. Chem.* **86**(9), 4115–4119 (2014).
161. E. W. Hislop *et al.*, "Label-free cytometric evaluation of mitosis via stimulated Raman scattering microscopy and spectral phasor analysis," *Anal. Chem.* **95**(18), 7244–7253 (2023).
162. M. Xue *et al.*, "Advancing living *Bacillus* spore identification: Multi-head self-attention mechanism-enabled deep learning combined with single-cell Raman spectroscopy," *J. Innov. Opt. Health Sci.* **19**(1), 2550030 (2026).
163. N. Burzynski *et al.*, "Deep learning techniques for unmixing of hyperspectral stimulated Raman scattering images," *2021 IEEE Int. Conf. Big Data (Big Data)*, pp. 5862–5864, IEEE (2021).
164. F. X. Xu *et al.*, "Discrimination of lipid composition and cellular localization in human liver tissues by stimulated Raman scattering microscopy," *J. Biomed. Opt.* **29**(1), 016008–016008 (2024).
165. S. Yan *et al.*, "Hyperspectral stimulated Raman scattering microscopy unravels aberrant accumulation of saturated fat in human liver cancer," *Anal. Chem.* **90**(11), 6362–6366 (2018).
166. K.-C. Huang *et al.*, "Multiplex stimulated Raman scattering imaging cytometry reveals lipid-rich protrusions in cancer cells under stress condition," *iScience* **23**(3), 100953 (2020).
167. B. Manifold *et al.*, "Imaging neurotransmitter transport in live cells with stimulated Raman scattering microscopy," arXiv:2205.05798.
168. F. Hu, L. Shi, W. Min, "Biological imaging of chemical bonds by stimulated Raman scattering microscopy," *Nat. Methods* **16**(9), 830–842 (2019).
169. M. Z. Vardaki, V. G. Gregoriou, C. L. Chochos, "Biomedical applications, perspectives and tag design concepts in the cell-silent Raman window," *RSC Chem. Biol.* **5**(4), 273–292 (2024).
170. S. Hong *et al.*, "Live-cell stimulated Raman scattering imaging of alkyne-tagged biomolecules," *Angew. Chem. Int. Ed.* **53**(23), 5827–5831 (2014).
171. S. Bakthavatsalam, K. Dodo, M. Sodeoka, "A decade of alkyne-tag Raman imaging (ATRI): Applications in biological systems," *RSC Chem. Biol.* **2**(5), 1415–1429 (2021).
172. W. J. Tipping *et al.*, "Temporal imaging of drug dynamics in live cells using stimulated Raman scattering microscopy and a perfusion cell culture system," *RSC Chem. Biol.* **3**(9), 1154–1164 (2022).

173. Y. Miao *et al.*, "9-Cyanopyronin probe palette for super-multiplexed vibrational imaging," *Nat. Commun.* **12**(1), 4518 (2021).
174. M. Andreana *et al.*, "Amplitude and polarization modulated hyperspectral stimulated Raman scattering microscopy," *Opt. Express* **23**(22), 28119–28131 (2015).
175. C. Guan, N. Zeng, H. He, "Review of polarization-based technology for biomedical applications," *J. Innov. Opt. Health Sci.* **18**(02), 2430002 (2025).
176. J. Fan *et al.*, "Generating bright-field images of stained tissue slices from Mueller matrix polarimetric images with CycleGAN using unpaired dataset," *J. Innov. Opt. Health Sci.* **18**(02), 2343003 (2025).
177. Y. Li *et al.*, "Pix2Pix-driven virtual pathology staining based on phase contrast microscopy: A low-cost strategy for rapid intraoperative assessment of breast cancer," *J. Innov. Opt. Health Sci.* **19**, 2540005 (2026).
178. T. C. Hollon *et al.*, "Rapid, label-free detection of diffuse glioma recurrence using intraoperative stimulated Raman histology and deep neural networks," *Neuro Oncol.* **23**(1), 144–155 (2021).
179. J. Ao *et al.*, "Stimulated Raman scattering microscopy enables Gleason scoring of prostate core needle biopsy by a convolutional neural network," *Cancer Res.* **83**(4), 641–651 (2023).
180. M. Mannas *et al.*, "Stimulated Raman histology interpretation by artificial intelligence provides near-real-time pathologic feedback for unprocessed prostate biopsies," *J. Urol.* **211**(3), 384–391 (2024).
181. Y. Yang *et al.*, "Histological diagnosis of unprocessed breast core-needle biopsy via stimulated Raman scattering microscopy and multi-instance learning," *Theranostics* **13**(4), 1342 (2023).
182. H. Ni *et al.*, "High-content stimulated Raman histology of human breast cancer," *Theranostics* **14**(4), 1361 (2024).
183. L. Ma *et al.*, "DeepLuAd: Semantic-guided virtual histopathology of lung adenocarcinoma via stimulated Raman scattering," *Theranostics* **16**(5), 2324 (2026).
184. X. Chen *et al.*, "Accurate and rapid detection of peritoneal metastasis from gastric cancer by AI-assisted stimulated Raman molecular cytology," *Adv. Sci.* **10**(21), 2300961 (2023).
185. Y. He *et al.*, "Deep learning enhanced label-free cervical screening via stimulated Raman cytology," *Talanta* **298**, 128982 (2025).
186. Y. Yang, L. Chen, M. Ji, "Stimulated Raman scattering microscopy for rapid brain tumor histology," *J. Innov. Opt. Health Sci.* **10**(05), 1730010 (2017).
187. L. Ma *et al.*, "Stain-free histopathology with stimulated Raman scattering microscopy," *Anal. Chem.* **96**(20), 7907–7925 (2024).
188. Y. Zhang *et al.*, "StainOptimizer: A whole-process evaluation approach with interpretability framework for optimizing virtual staining methods," *J. Innov. Opt. Health Sci.* **19**, 2650009 (2026).
189. X. Zhang *et al.*, "Phototoxic effects of nonlinear optical microscopy on cell cycle, oxidative states, and gene expression," *Sci. Rep.* **12**(1), 18796 (2022).
190. B. Manifold, D. Fu, "Quantitative stimulated Raman scattering microscopy: Promises and pitfalls," *Annu. Rev. Anal. Chem.* **15**(1), 269–289 (2022).
191. L. Zhang *et al.*, "Label-free imaging of hemoglobin degradation and hemosiderin formation in brain tissues with femtosecond pump-probe microscopy," *Theranostics* **8**(15), 4129 (2018).
192. H. Lin, J.-X. Cheng, "Computational coherent Raman scattering imaging: Breaking physical barriers by fusion of advanced instrumentation and data science," *eLight* **3**(1), 6 (2023).
193. D. Tsikritsis, E. J. Legge, N. A. Belsey, "Practical considerations for quantitative and reproducible measurements with stimulated Raman scattering microscopy," *Analyst* **147**(21), 4642–4656 (2022).
194. G. S. Collins *et al.*, "TRIPOD+ AI statement: Updated guidance for reporting clinical prediction models that use regression or machine learning methods," *BMJ* **385**, e078378 (2024).
195. K. Luo *et al.*, "Coherent nonlinear vibrational microscopy," *Appl. Phys. Rev.* **13**(2), 021329 (2026).